

Localization of Small Leakages in Water Distribution Networks using Concept Drift Explanation Methods*

Valerie Vaquet^{ID ‡} Fabian Hinder^{ID †} Kathrin Lammers
Jonas Vaquet Barbara Hammer^{ID}

Bielefeld University - Cognitive Interaction Technology (CITEC)
Inspiration 1, 33619 Bielefeld - Germany

October 25, 2023

Abstract

Facing climate change the already limited availability of drinking water will decrease in the future rendering drinking water an increasingly scarce resource. Considerable amounts of it are lost through leakages in water transportation and distribution networks. Leakage detection and localization are challenging problems due to the complex interactions and changing demands in water distribution networks. Especially small leakages are hard to pinpoint yet their localization is vital to avoid water loss over long periods of time. While there exist different approaches to solving the tasks of leakage detection and localization, they are relying on various information about the system, e.g. real-time demand measurements and the precise network topology, which is an unrealistic assumption in many real-world scenarios. In contrast, this work attempts leakage localization using pressure measurements only. For this purpose, first, leakages in the water distribution network are modeled employing Bayesian networks, and the system dynamics are analyzed. We then show how the problem is connected to and can be considered through the lens of concept drift. In particular, we argue that model-based explanations of concept drift are a promising tool for localizing leakages given limited information about the network. The methodology is experimentally evaluated using realistic benchmark scenarios.

Keywords: Water Distribution Networks · Leakage Localization · Automated Data-Analysis · Concept Drift · Explainable AI · Model Based Drift Explanations.

1 Introduction

Clean and safe drinking water is a scarce resource in many areas. Almost 80% of the world’s population is classified as having high levels of threat in water security [1].

*Funding in the frame of the ERC Synergy Grant “Water-Futures” No. 951424 is gratefully acknowledged.

†Authors contributed equally

‡Corresponding Author

This will aggravate in the future as due to climate change the already limited water resources will become more restricted [2]. Currently, across Europe, considerable amounts of drinking water are lost due to leakages in the system¹. The issue has been identified by the European Union, which put the topic on the political agenda recently².

In order to ensure a reliable drinking water supply, there is a need for reliable, safe, and efficient water distribution networks (WDNs). In addition to avoiding water losses, a crucial requirement is to ensure the quality of the drinking water, e.g. to avoid the spreading and growth of bacteria and other contaminants. Leakages pose a major risk to water quality as they make it possible for unwanted substances to enter the water system. Thus, monitoring the system for leakages is an efficient tool to avoid water loss and contamination [3].

Due to complex network dynamics and changing demand patterns detecting and localizing leakages are challenging tasks. This is aggravated by the fact, that the available data is very limited [4]. Usually, the precise network topology remains unknown or the documentation contains errors. As smart meter technologies are not widely distributed there is no real-time demand information [5]. This leaves a set of scarce pressure and possibly flow measurements. When considering historical recordings the presence and exact timings of possible leakages are frequently unknown as especially smaller leakages might not have been detected.

Detecting and localizing small leakages are particularly hard tasks as the changes induced by this anomaly easily get lost in the complex dynamics of the system as visualized in Figure 1. However, detecting small leakages is of particular relevance, as water losses and potential contamination over extended time periods are expected [6]. In contrast, larger leakages are usually detected more easily by monitoring tools or other means. For example, they are exposed to water accumulating in streets and are usually repaired within a short time window resulting in less water loss in total.

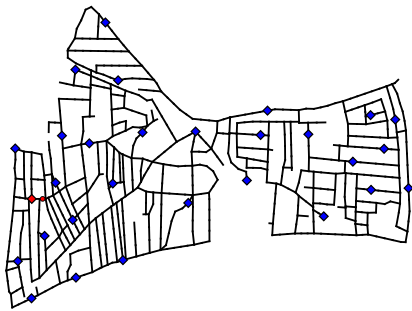
Many of the schemes for leakage detection and localization are based on building a hydraulic model replicating a specific system. This requires a lot of problem-specific information like the precise network topology and real-time demands [7, 4]. This strongly limits the applicability and generalization of current solutions as frequently this information is not available. Besides, whenever the real system changes the need to adapt the simulation arises. Recently, considerable research on applying machine learning techniques to leakage detection has been conducted [8, 9]. However, machine learning approaches tackling the task of leakage localization are still limited and frequently rely on network topologies and historic leakage-free data [4].

In this work, we analyze leakages in water distribution systems closer. We describe the WDN and potential leakages utilizing dynamic Bayesian Networks and thereof derive a definition for leakage detection and localization. Based on this we propose to apply a model-based drift explanation as an efficient tool for localizing small leakages given limited data.

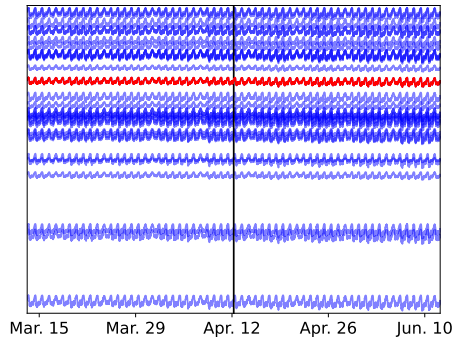
This paper is structured as follows. First, a brief introduction to WDNs and leakage detection, and an overview of the related work are provided (Section 2). Afterward, in Section 3 we model leakage detection in WDNs utilizing dynamic Bayesian networks and propose a formal definition of leakage detection and localization based on our modeling. Based on this we derive the proposed methodology (Section 4). Finally, we conclude our paper by presenting an experimental evaluation of the proposed model-based drift explanation methodology for leakage localization (Section 5) and discussing our findings (Section 6). The ethical considerations can be found in

¹<https://www.eureau.org/resources/publications/1460-eureau-data-report-2017-1/file>

²<https://eur-lex.europa.eu/legal-content/EN/TXT/HTML/?uri=CELEX:32020L2184&from=ES>



(a) L-Town topology. Diamonds mark the position of pressure sensors, red dot marks the leakage position.



(b) Pressures at sensors in Figure 1a (colors match), black line marks occurrence time of leakage.

Figure 1: L-Town topology and pressure value example. Small leakages cannot be found by the human eye even if highlighted.

Section 7.

2 Leakage Detection in Water Distribution Networks

This section briefly discusses how WDNs are usually modeled, and which network benchmarks are available. Besides, it introduces the standard monitoring setup and summarizes the body of related work on leakage detection and localization.

2.1 Water Distribution Networks

Water supply networks can be modeled as graphs consisting of nodes representing junctions and undirected edges representing pipes as the flow direction of the water is not pre-defined and can change over time due to different inputs and demands in the network. As usually real-world water supply systems are extended over time, changes in the network need to be expected [10]. In real-world networks, usually, there are some information gaps in the knowledge of the exact topology and additional information. For example, the exact diameters of certain pipes are frequently unknown and elevation levels within the network are rarely measured due to the associated cost [11].

Water systems are increasingly equipped with sensor technologies. Sensors can be installed at the connections of the pipes or in basins (e.g. level or pressure sensors) or in the pipes (e.g. flow sensors). While it is also possible to measure the demand of the end-users by so-called smart meters, usually this is not done exhaustively due to the associated cost and privacy concerns [5].

As collecting real-world data with ground truth is not possible since there is no exact knowledge of the properties of real-world leakages (e.g. exact onset times), usually monitoring algorithms are fitted and evaluated on simulation data. A common choice for simulating network hydraulics and anomalous behavior like leakages and sensor faults is the EPANET simulator [12] which is yielding a steady-state simulation of the network hydraulics.

One popular network used for evaluating anomaly detection algorithms is the L-Town network which resembles parts of the old town of Limassol, Cyprus. It is a comparably complex and realistic water supply network. As realistic demands for a

period of two years are available, one can simulate different leakage scenarios using EPANET. As visualized in Figure 1. Area A contains 661 nodes and 764 edges with 29 optimally placed pressure sensors [7].

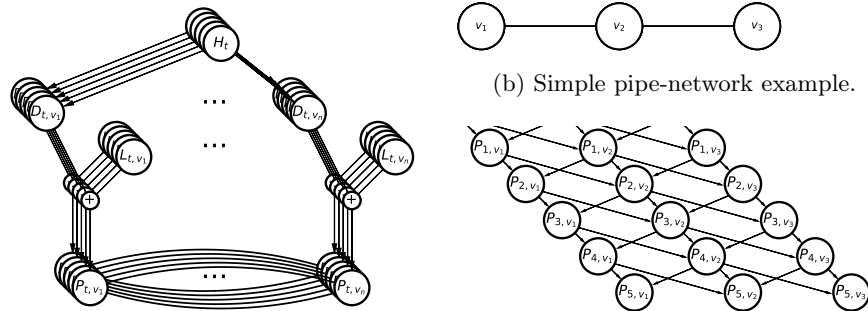
2.2 Leakage Detection

As discussed before, detecting and localizing leakages is of particular relevance for both reducing water loss and minimizing contamination risks. Handling leakages is usually done by implementing monitoring systems which are commonly split into the following sub-tasks [3, 13]: First, anomalies need to be *detected*, i.e. an alarm should be raised whenever there is atypical behavior in the system. In the second step, more information about the anomalous event is collected. The goal is to *localize* the leakage position and determine its size and possibly its exact starting time. Finally, some kind of accommodation is required. In case a leakage has been found and localized, it might be necessary to temporarily interrupt water flow in the area of the leakage and to repair the leaking pipe.

There are two main methodological groups to attempt leakage detection and localization. While traditionally the tasks are approached using hydraulic modeling of the systems, with increasing availability of (real-time) sensor data more machine learning-based approaches are used [8, 9, 4]. For the detection step, the majority of approaches is relying on a prediction residual strategy, e.g. [14, 15, 16, 17, 18, 19, 20]. The overarching scheme is to model leakage-free operation employing hydraulic or machine learning-based approximations and to compare the model to the sensor readings. In case of a large discrepancy, a leakage alarm is triggered [4]. There are also some approaches that perform some kind of comparison to historical recordings to detect anomalous behavior, e.g. [21, 22, 23]. End-to-end machine learning approaches are very limited due to large networks, complex dynamics, and limited and imbalanced data [4].

Leakage localization is usually solved as an inverse problem by hydraulic-based approaches, e.g. [14, 15, 16, 17, 18]. Basically, the leakage is localized by minimizing the discrepancy over different simulated leakage locations. Note that this methodology requires knowledge of the exact topology and is computationally expensive as a high number of simulations need to be computed. To our knowledge machine learning-based approaches to leakage localization are very scarce [4]. [24] propose to localize leakages by a geometric comparison to historical leakage-free data and apply a graph-based interpolation as a pre-processing step. [19] rely on evolutionary polynomial regression to approximate the network dynamics and analyze the flow rate in a residual-based manner.

In summary, the current state of the art relies on very precise information about the network topology. Especially hydraulic-based approaches frequently assume real-time demand information while machine learning-based works tend to require considerable periods of (leakage-free) data recordings for training. These assumptions can frequently not be met. However, incorporating that much information into building a methodology might be not desirable as it limits the generalization to different network topologies, e.g. different water networks or adaptations of existing networks. This restricts the applicability of these important technologies to many use cases while finding solutions is crucial considering increasing water scarcity. Additionally, the hydraulics-based approaches suffer from long simulation times. Before proposing our approach to leakage localization which is solely relying on the measured stream of pressures and does not require any knowledge of the network topology in Section 4, we will first formalize and analyze the impacts of leakages in WDNs in the next section.



(a) Complete dynamic Bayesian network. (c) Dynamic Bayesian sub-network for Stacked circles indicate temporal self-dependency (compare Figure 2c). (b) Simple pipe-network example. (c) Dynamic Bayesian sub-network for Stacked circles indicate temporal self-dependency of the pipe network presented in Figure 2b.

Figure 2: Visualization of the modeling by a dynamic Bayesian network.

3 A Causal Model for Water Distribution Networks

A common way to model and get a better understanding of complex dynamic systems is by using a *dynamic Bayesian network* [25, 26]. Modeling conditional dependencies of a set of variables over time using a directed acyclic graph, Bayesian networks [26, 27] constitute a suitable tool to model the dynamics in WDNs and the influence of leakages.

In the case of WDNs, we can rely on the structure of the network G and model pipes as edges and their connecting points as nodes. We will first describe a Bayesian network describing a leakage-free system and then discuss its extensions to scenarios containing leakages. As visualized in Figure 2 at each node $v \in V(G)$ we observe a *pressure* $P_{t,v}$ at each time step t . Each pressure measurement $P_{t,v}$ depends on the pressures at time $t - 1$ of the considered node and its neighborhood, i.e. $P_{t-1,v}$, and $P_{t-1,w}$ where $w \in N_G(v)$ is a direct neighbor of v in G . Besides, the pressure $P_{t,v}$ additionally depends on the *demand* at the respective position and time $D_{t,v}$. The demands in turn are independent of each other but each demand $D_{t,v}$ depends on its respective past $D_{t-1,v}, D_{t-2,v}, \dots$. Besides, all demands depend on an additional *hidden cause* H_t which models outer circumstances like the weather or public holidays. The hidden cause only depends on its history, i.e. H_{t-1}, H_{t-2}, \dots .

Additionally modeling leakages in the system can be accomplished by introducing additional leakage demands as commonly done in the literature, e.g. [14]. In our network, $L_{t,v}$ models the water loss through possible *leakages* at every node $v \in V(G)$. Leakages only depend on the time t . Introducing leakage to the system additionally introduces a dependency of the pressure $P_{t,v}$ on $L_{t,v}$ for each node v .

Notice that though we made use of discrete-time to make things easier, we can assume that $P_{t,v}$ is obtained by a set of differential equations and thus get a good approximation using a sufficiently small time step size.

A common way to express the interplay of the variables functionally is to rely on the formalism of *functional Bayesian networks* [27, 28]. Given an underlying graph (including time) N , the value X_n of node $n \in V(N)$ can be computed using a deterministic function f_n that takes the values $X_{\text{Pa}(n)}$ of the parents of n in N and independent noise ε_n , i.e. we have $X_n = f_n(X_{\text{Pa}(n)}, \varepsilon_n)$ [28]. Since in water distribution systems the underlying physics describing the interplay of the components do not change over time, in this setting assuming that the function f_n does not depend on time, i.e. if n and n' represent the same node up to time then $f_n = f_{n'}$ is reasonable.

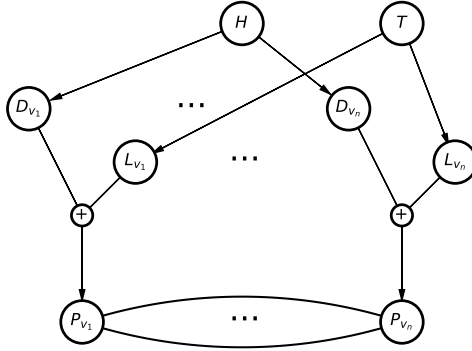


Figure 3: Illustration of simplified Bayes network presented in Figure 2a

Thus for the water system, we obtain a function $P_v : \mathbb{R}^{N_G(v) \cup \{v\}} \times \mathbb{R} \times \mathbb{R} \rightarrow \mathbb{R}$ for every node v in the water network G that computes the pressure of the next time-step using the last pressures and the current demand, i.e. $P_{t,v} = P_v((P_{t-1,w})_{w \in N_G(v) \cup \{v\}}, D_{t,v} + L_{t,v}, \varepsilon_{v,t})$. For reasons of simplicity, we will assume that the behavior of the pressures given the demands is mainly deterministic, i.e. P_v is invariant with respect to $\varepsilon_{v,t}$ for all v . Notice that both pressure and demand can be modeled using a single real number for each node in this setup. However, replacing those with a vector, e.g. to additionally consider flow speed, chloride concentration, etc., is straightforward.

Using this setup we can now formally define the problem of leakage detection and localization. As the size of the leakages is described using additional demands $L_{t,v}$ at node v it is reasonable to assume that $L_{t,v} \geq 0$ and $L_{t,v} > 0$ indicates a leakage at node v . Thus, the leakage at node v gets worse/grows if it is strictly larger in the next time-step, i.e. $L_{t,v} < L_{t+1,v}$, and a new leakage appears if the leakage was 0 before, i.e. $L_{t,v} = 0 < L_{t+1,v}$. Thus, we can formalize leakages and thus leakage detection and localization as the following problem:

Definition 1. We say that a *leakage occurs* at node v and time t if $L_{t-1,v} < L_{t,v}$. The task of *leakage detection* refers to the problem to determine whether there occurs a leakage at time t , i.e. determine the set $\{t \mid \exists v \in V(G) : L_{t-1,v} < L_{t,v}\}$. The task of *leakage localization* refers to the task to determine whether there occurs a leakage at node v , i.e. determine the set $\{v \mid \exists t : L_{t-1,v} < L_{t,v}\}$.

4 Methodology

Based on the formalization of the problem which we provided in the prior section, we now discuss how leakage detection and localization can be accomplished relying on the notion of concept drift.

4.1 Leakage Detection

Considering the dynamics in the WDN over longer periods, only the occurrence of leakages strongly depends on the time. While demands are ever-changing they tend to follow relatively stable patterns, which will average out over longer time periods. Thus, we propose to simplify the network which we proposed in Section 3 and visualized in Figure 2 to a *standard Bayesian network* [27, 28]. As can be seen in Figure 3, we have to introduce a random variable T that represents time to model the strong

time dependency of the leaks. We replace H_t by H , $D_t | H_t$ by $D | H$ and L_t by the sub-network $T \rightarrow L$ with the property $\mathbb{P}_{L|T=t} = \mathbb{P}_{L_t}$.

Looking at the resulting dependencies in our modeling it becomes apparent that leakages are the only variables that depend on time. Besides, they directly influence the pressures. Thus, changes in L_v , e.g. the onset of a leakage, are reflected in the stream of pressure measurements. An established way to describe such a phenomenon is the notion of *concept drift* or drift for shorthand. While commonly drift is defined as change in the data generating distribution [29], on a statistical level it makes sense to consider a general statistical interdependence of data and time via a distribution \mathcal{D} on $\mathcal{T} \times \mathcal{X}$ which decomposes into a distribution \mathbb{P}_T in time-domain \mathcal{T} and the conditional distributions \mathcal{D}_t on data-space \mathcal{X} [30]. One of the key findings of [30] is a unique characterization of the presence of drift as a statistical dependency of time T and data X if a time-enriched representation of the data $(T, X) \sim \mathcal{D}$ is considered, i.e. \mathcal{D}_t has no drift if and only if $X \perp\!\!\!\perp T$.

The task of determining whether or not there is drift during a time period, referred to as *drift detection* thus directly aligns with detecting leakages in the considered setup. Numerous approaches for drift detection exist in the body of literature [29]. Many of the residual-based leakage detection approaches which were briefly discussed in Section 2.2 are implementing supervised drift detection which is relying on model loss as a proxy for drift in the underlying distribution.

4.2 Leakage Localization

So far, we argued that leakages can be formalized as drift. Leakage detection can be accomplished by means of drift detection, as frequently implicitly done in related work. However, as discussed before, a second mandatory step in a monitoring system is to localize the leakage, i.e. to pinpoint its exact location. We will analyze this task from the perspective of drift. However, before obtaining a promising methodology for leakage localization, we need to first analyze the given setup a bit further.

4.2.1 Analyzing the Effect of Leakages in the System

As each P_v computes the pressure at every single node, we can easily combine those and end up with a map that updates the pressures of the entire network $P : \mathbb{R}^{V(G)} \times \mathbb{R}^{V(G)} \rightarrow \mathbb{R}^{V(G)}$, $P_t = P(P_{t-1}, D_t + L_t)$, where we suppress the node-index to indicate that we consider all nodes of the same type at once, i.e. $P_t = (P_{t,v})_{v \in V(G)}$ and analogous for D_t and L_t . Here, t represents a mere index of a time-series, other than before it has no statistical meaning.

The function P models one step in a simulation. Commonly this is done using steady-state simulations [12]. Therefore, it is reasonable to believe that for the same demands, the pressure values become more similar in the next time-step, i.e. $\|P(P_1, D) - P(P_2, D)\|_1 < \|P_1 - P_2\|_1$. Formally this can be expressed by the notion of Lipschitz continuity with constant < 1 . Conversely, under the Lipschitz assumption, the dynamics in the system become a steady state. Indeed, we can show that the pressure values do not depend on initial pressures but on the demands alone, as one would intuitively expect (see appendix, Lemma 1).

Furthermore, it is also reasonable that a small change in demand at one node will for a single time step result in a small change of pressures at that node only, i.e. is continuous. A type of continuity that is commonly used when dealing with differential equations is α -Hölder continuity which is given by $|P_v(P, D_1) - P_v(P, D_2)| \leq C|D_1 - D_2|^\alpha$ for some constants $C > 0$ and $0 < \alpha \leq 1$. Under this assumption, we can show

that the entire pressure dynamics depend continuously on all input demands. Details can be found in the appendix (see Lemma 2).

As a consequence, we can make statements about the mean pressures: when considering demands over a longer period of time we observe that the oscillations cancel out. Under our assumptions, this effect propagates through to the pressures, i.e. the cancellation also occurs in the pressures. Since the fluctuation usually causes some problems, data analysis is commonly performed using such mean values over time windows. In this case, we can show that the effect of a leakage decays exponentially fast though-out the network. Formally this can be stated as follows:

Theorem 1. *Assume that the transition function P is Lipschitz continuous in the first and α -Hölder continuous second argument, i.e. $\|P(p, d) - P(p', d')\|_1 \leq C_s \|p - p'\|_1 + C_d \|d - d'\|_1$. Let $D \in \mathbb{R}^{V(G)}$ be a constant/mean demand pattern and $L \in \mathbb{R}^{V(G)}$, $L_w = \delta_{vw} l$, $l > 0$ be a leak at node v . If $C_s < 1/(\deg G + 1)$, where $\deg G = \max_{u \in V(G)} |N_G(u)|$ is the maximal node degree in G , then the effect of the leakage decays exponentially throughout G :*

$$|(P(D))_w - (P(D + L))_w| \begin{cases} = 0, & d_G(w, v) = \infty \\ < \frac{C_d l^\alpha \cdot (C_s (\deg G + 1))^{d_G(v, w)}}{1 - C_s (\deg G + 1)}, & \text{otherwise} \end{cases}$$

where $d_G(u, v)$ denotes the distance in G , i.e. the length of the shortest path in G connecting u and v or $= \infty$ if there is no such path.

The assumption $C_s < 1/\deg G$ is necessary to assure a monotonic decrease of the effect.

Proof. Due to space restrictions, the proof can be found in the appendix. \square

4.2.2 Baseline Methodology for Leakage Localization

Combining our findings from modeling leakages in WDNs (Figure 3) and Theorem 1, we obtain that leakages can be modeled as a drift in the system which inflicts itself locally much stronger than globally as the effect of the leakage on the pressure measurements decays exponentially. This observation gives rise to a very simple window-based leakage localization technique:

$$v_{\text{leakage}}(t; w) := \arg \max_{v \in V(G)} \left| \sum_{i=t-w}^t P_{i,v} - \sum_{i=t}^{t+w} P_{i,v} \right| \quad (1)$$

where t is the onset time of the leakage, which can be obtained by drift detection, and w is the window size, a hyper-parameter of this method.

While this simple methodology is justified by the theory we expect some shortcomings when applying it to realistic data. For example, just considering the discrepancy in the mean does not account for differences in the variance across different sensor nodes. Therefore, we propose to again consider the problem through the lens of drift.

4.2.3 Model-Based Drift Explanations for Leakage Localization

To localize leakages we need to accumulate additional knowledge on the drift. More precisely, we aim to identify which area of the network is most affected by the drift as according to our prior arguments this will be the area containing the leakage. There are different approaches to analyzing drift as nicely summarized in [31, 32]. However, they cannot be used in an automated procedure. In contrast, [32, 33] proposes a

model-based drift explanation scheme which seems to be a promising choice for solving our leakage localization task when used with feature-based explanation schemes.

The main idea of model-based explanations is to reduce the problem of explaining drift to explaining a suitably trained model [31, 32]: As pointed out by [30, 32] drift is encoded in the dependence of X and T . Thus, by training a model $h(t | x)$ to estimate $\mathbb{P}[T = t | X = x]$ we essentially extract information about the drift. Given the time of the drift which can be obtained by applying drift detection as discussed in Section 4.1, we can train a simple binary classifier discriminating between samples from before and after the drift. While [31, 32] presented how this idea can be combined with a range of local and global explanation techniques which were considered for the specific task of feature selection in [33], due to the results of Theorem 1 we argue that for the considered use case feature-based explanation schemes are of particular relevance. As we discussed leakages mainly affect the pressure measurements which are close to the leakage location, we assume that these are the most important features when training a discriminator. A linkage between these two ideas as well as the Bayesian modeling described in Section 3 (Figure 3) was provided in [33].

Model-based drift explanations are not limited to the case in which the exact time of the drift or in our case the onset of leakage is a prerequisite. In this case drift segmentations [34] can be used to implicitly find the drift. As pointed out by [32] this can be done by multi-regression tasks aiming to fit polynomial or Fourier-transformed time [35, 36] can be used as a model which can be explained by different explanation schemes. This might be of particular relevance in case of considerable delays of the drift detection mechanisms in realistic applications.

In the remainder of the paper, we will experimentally evaluate the suitability of both versions of model-based drift explanations. We will consider different instantiations of feature-based explanation schemes and the previously discussed baseline approach of moving windows.

5 Experiments

Before presenting and discussing the results we will briefly introduce the experimental setup and evaluation³.

5.1 Setup, Data, and Metrics

5.1.1 Data Generation

To obtain expressive results we simulate our own scenarios for the experimental evaluation. We rely on the L-Town network which we introduced in Section 2. In addition to the fact that it models a realistic WDN, realistic demand data for a period of two years is publicly available [7]. For simulating the data, we use the atmn toolbox⁴ and rely on the optimal placement of pressure sensors as in [7]. We consider a leakage size of 0.007mm which would be categorized as small background leakages in the L-Town network and poses challenges to many approaches in the literature [7, 4]. All scenarios contain data of a real-time length of two months with a sampling density of 15-minute intervals with the leakage present in the second half of the scenario. We consider all 764 pipes. As the amount of available realistic demands is limited and the simulation is deterministic we use an offset of 15 days between two scenarios to

³The code of the experiments will be made available after acceptance.

⁴<https://pypi.org/project/atmn/>

have a sufficiently large amount of data for statistical analysis, leading to 42 runs per pipe.

5.1.2 Used Methods

In our experiments, we consider the setup where the drift time is available and where it is not (w/o DD). In addition to a random baseline (Random), where a node is selected at random, and the mean strategy (Mean) according to Theorem 1, where the node with the maximal feature-wise divergences of mean-values before and after the leakage is selected (see Eq. 1), we use the following instantiations of model-based drift explanations: We combine tree-based models (RandomForests (RF) and ExtraTrees (ET)) with feature importance (FI) and Permutation Feature Importance (PFI). Besides, we consider linear models with different regularization (Logistic Regression with l1 (LogR (l1)), l2 (LogR (l2)), parameters are automatically determined by cross-validation, and linear SVM (SVM)). Here we consider the absolute value of the weight vector as the importance score.

5.1.3 Metrics

In the following let $s^* \in S$ denote the node selected by the respective method and by $v \in V(G)$ the leaky node. We make use of four metrics: distance between selected and actual node (distance; $d(s^*, v)$), number of nodes in S closer to the actual node (#closer; $|\{s \in S \mid d(s, v) < d(s^*, v)\}|$), and relative distance between actual node, selected and optimal node (rel. dist.; $d(s^*, v) / \min_{s \in S} d(s, v)$, we exclude the cases where $v \in S$ to avoid division by 0) which is normalized in contrast to the simple distance and smooth in contrast to the closer node metric, and the intersection size of the 3 most important and closest sensors (best-3) which is relevant for interpolation tasks.

For d we consider the following distances: the topological distance (topo.) in the graph G , i.e. the number of nodes of the shortest connecting path, and the actual geographic distance (geo.). We also documented model accuracy.

5.2 Results

When analyzing the obtained results, we found that the values when computed topological and geographical distance differ neither quantitatively, i.e. in the absolute number obtained, nor qualitatively, i.e. with respect to the ranking of the methods. The only exception is the distance metric, which does differ quantitatively, only, which is to be expected. Therefore, we will not distinguish the cases for the distance measures in the following and only present the results for the topological distance.⁵

Our results are summarized in Table 1 and Figure 4. As can be seen, there is a strong correlation between distance, #closer, and rel. dist., which we were able to confirm by a range of statistical tests. We find that the simple Mean baseline performs significantly better than the random baseline as suggested by Theorem 1. However, the explanation-based leakage localization schemes are capable of pinpointing the leakage even closer. An explanation for this is that the linear models compensate for variance and covariance terms. To see this, consider the two mean values of the Mean approach as prototypes that induce a linear model, which typically suffers from this problem.

⁵The full results for geographical distance as well as additional visualization of all metrics are provided in the appendix.

Table 1: Results of models for different metrics using topological distances. The table shows the median (m), mean (μ), and standard deviation (σ) over all 764 nodes and 42 runs. Bigger better (+), smaller better (-).

method	distance (-)		#closer (-)		rel. dist. (-)		best-3 (+)	
	m	$\mu\pm\sigma$	m	$\mu\pm\sigma$	m	$\mu\pm\sigma$	m	$\mu\pm\sigma$
Random	27	29.70 \pm 16.85	14	13.94 \pm 8.36	6.5	9.47 \pm 9.76	0	0.31 \pm 0.51
Mean	17	18.97 \pm 12.83	7	8.01 \pm 6.38	3.8	5.84 \pm 6.56	1	0.70 \pm 0.77
FI (RF)	5	5.09 \pm 4.04	0	0.51 \pm 1.73	1.0	1.18 \pm 1.21	1	1.24 \pm 0.50
FI (ET)	5	5.03 \pm 3.80	0	0.48 \pm 1.59	1.0	1.17 \pm 1.24	2	1.81 \pm 0.63
PFI (RF)	5	5.03 \pm 3.50	0	0.47 \pm 1.33	1.0	1.15 \pm 0.82	1	1.28 \pm 0.52
PFI (ET)	5	5.00 \pm 3.45	0	0.46 \pm 1.34	1.0	1.16 \pm 1.10	2	1.86 \pm 0.64
SVM	5	9.72 \pm 13.67	0	3.29 \pm 7.82	1.0	2.38 \pm 4.23	2	1.49 \pm 0.78
LogR (l2)	7	14.54 \pm 14.56	1	6.30 \pm 8.59	1.2	4.02 \pm 5.55	1	1.23 \pm 0.96
LogR (l1)	6	13.82 \pm 15.08	1	5.75 \pm 8.66	1.0	3.80 \pm 5.70	1	1.18 \pm 0.88
FI (RF w/o DD)	5	10.18 \pm 12.97	0	4.20 \pm 8.29	1.0	2.31 \pm 3.38	1	0.99 \pm 0.55
FI (ET w/o DD)	5	8.04 \pm 10.55	0	2.64 \pm 6.82	1.0	1.79 \pm 2.50	1	1.26 \pm 0.68
PFI (RF w/o DD)	5	5.99 \pm 5.79	0	1.12 \pm 3.07	1.0	1.34 \pm 1.11	1	1.10 \pm 0.49
PFI (ET w/o DD)	5	10.94 \pm 11.23	0	4.30 \pm 6.58	1.0	2.43 \pm 2.71	1	0.76 \pm 0.52

While in the median all tree-based methods find the closest sensor node, the experiments with logistic regression tend to find sensors that are slightly further away from the leakage. This ranking can also nicely be seen in the box plots in Figure 4b and be confirmed by statistical tests. This might be a reflection of the fact that linear models are unable to learn the more complex, non-linear relationships between features which explain the tree-based models outperform them if information about the drift is provided.

Besides, we find that the experiments without drift detection extract relevant information about the drift, although with less precision. This is to be expected as the training involves the additional complication of recognizing the drift. However, we consider the results to be very promising.

Considering the best-3-metric, we find that even the best performing tree-based implementations are only identifying less than 2 of the closest sensor nodes when considering the top 3 feature importances. This needs further investigation in future work.

In addition to the global investigation, figuring out whether there are areas that pose particular challenges to the methodology is interesting and might generate insights. Therefore we additionally created a visualization of the results for some selected methods (see Figure 5). The maps show the distance between the leakage and the selected sensor node. The values are pipe-wise normalized taking on values between the theoretically closest and the mean for the Random baseline. As can be seen, the error distribution is not uniform but rather depends on the location in the network. Though it is influenced by the model (and the metric as further analysis shows) certainty tendencies and error hot spots can be observed across all setups. On closer consideration, we can attribute at least some of those effects to properties of the network, like sensor density, number of junctions, or type of network parts (like tanks). However, we were yet not able to fully find the actual reason for this effect. Thus, further research on our agnostic approach is necessary.

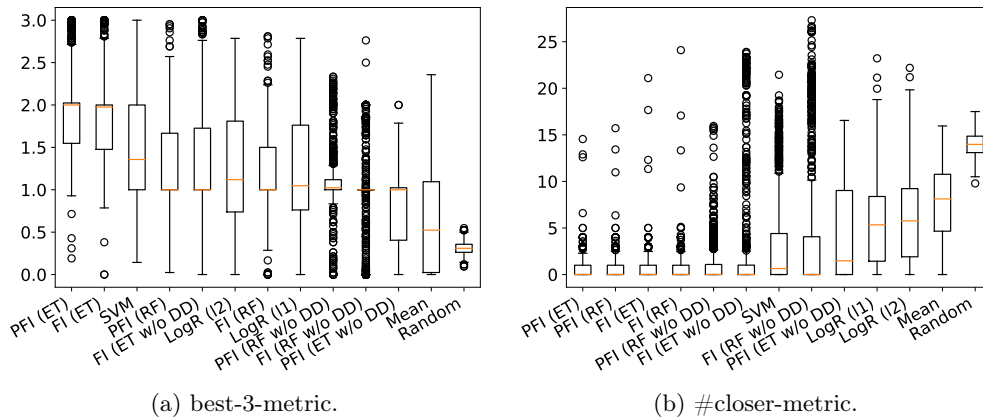


Figure 4: Visualisation of results (on mean per pipe) for best-3- and #closer-metric using geographic distances. Every point corresponds to the mean over all runs on a single pipe. Ordering is according to mean (best to worst: left to right).

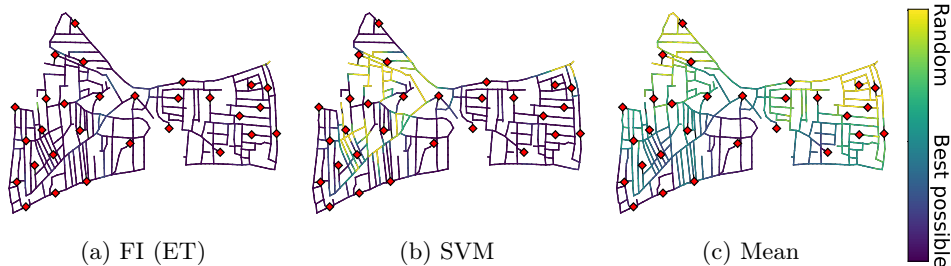


Figure 5: Visualisation of (relative) distance between pipe and selected node. Value is normalized between best possible value (closest sensor; purple) and Random baseline (yellow). Red diamonds mark sensor positions.

6 Discussion

In this contribution, we worked on the task of leakage localization which is of particular societal relevance as drinking water is an increasingly limited resource due to climate change. To the best of our knowledge, this is the first work analyzing the dynamics of WDNs utilizing Bayesian networks. We obtained that concept drift is a valid way to model leakages in WDNs and that the influence of leakages decays exponentially fast. Based on these insights we obtained an approach relying on model-based drift explanations which showed promising first results in our experimental evaluation even though we considered small leakages which are generally hard to localize. In contrast to established work, our methodology has two main advantages. First, it is independent of the network’s topology and does not require any additional data except for pressure measurements. Thus, it is applicable in many real-world scenarios where data is limited and capable of generalizing over different network topologies. Second, it is computationally lightweight in comparison to hydraulic-based approaches which rely on fitting critical parameters and running many computationally expensive simulations at inference time.

While the methodology we experimented with was a suitable tool to find the closest sensor node for tree-based implementations, this still leaves considerable regions of pipes as candidates for the leakage locations due to little sensor availability in the

network. Future work could investigate whether using virtual sensors as a proxy for the pressures, e.g. [37], at nodes without sensors could work out. Considering the difficulties all implementations shared in some areas, incorporating water experts for further analysis might be valuable.

7 Ethics

This work uses publicly available benchmark data and did not carry out any user studies. The contribution attempts to solve the crucial problem of leakage detection and localization on minimal information. Thus, this application for the societal good even works on reducing the amount of possibly critical information necessary while reducing computation times and thus energy demands. To the best of our knowledge, we cannot see how this methodology can be used for harmful applications.

References

- [1] Charles J Vörösmarty et al. “Global threats to human water security and river biodiversity”. In: *nature* 467.7315 (2010), pp. 555–561.
- [2] Matthew Rodell et al. “Emerging trends in global freshwater availability”. In: *Nature* 557.7707 (2018), pp. 651–659.
- [3] Demetrios G. Eliades and Marios M. Polycarpou. “A Fault Diagnosis and Security Framework for Water Systems”. In: *IEEE Transactions on Control Systems Technology* 18.6 (Nov. 2010), pp. 1254–1265. ISSN: 1558-0865. DOI: 10.1109/TCST.2009.2035515.
- [4] Valerie Vaquet et al. “Machine Learning Challenges in Water Distribution Networks - a Survey and a Graph Neural Network-based Solution for Leakage Detection and Localization”. In: 2023. URL: <https://pub.uni-bielefeld.de/record/2977930>.
- [5] Rachel Cardell-Oliver and Harrison Carter-Turner. “Activity-Aware Privacy Protection for Smart Water Meters”. In: *Proceedings of the 8th ACM International Conference on Systems for Energy-Efficient Buildings, Cities, and Transportation*. BuildSys ’21. Coimbra, Portugal: Association for Computing Machinery, 2021, 31–40. ISBN: 9781450391146. DOI: 10.1145/3486611.3486650. URL: <https://doi.org/10.1145/3486611.3486650>.
- [6] A. Lambert. “Accounting for Losses: The Bursts and Background Concept”. en. In: *Water and Environment Journal* 8.2 (Apr. 1994), pp. 205–214. ISSN: 1747-6585, 1747-6593. DOI: 10.1111/j.1747-6593.1994.tb00913.x. URL: <https://onlinelibrary.wiley.com/doi/10.1111/j.1747-6593.1994.tb00913.x> (visited on 03/31/2023).
- [7] Stelios G. Vrachimis et al. “Battle of the Leakage Detection and Isolation Methods”. EN. In: *Journal of Water Resources Planning and Management* 148.12 (Dec. 2022), p. 04022068. ISSN: 1943-5452. DOI: 10.1061/(ASCE)WR.1943-5452.0001601. URL: <https://ascelibrary.org/doi/10.1061/%28ASCE%29WR.1943-5452.0001601> (visited on 10/06/2022).
- [8] Chengyu Hu et al. “A survey on sensor placement for contamination detection in water distribution systems”. en. In: *Wireless Networks* 24.2 (Feb. 2018), pp. 647–661. ISSN: 1572-8196. DOI: 10.1007/s11276-016-1358-0. URL: <https://doi.org/10.1007/s11276-016-1358-0> (visited on 10/26/2022).

- [9] Yipeng Wu and Shuming Liu. “A review of data-driven approaches for burst detection in water distribution systems”. In: *Urban Water Journal* 14.9 (Oct. 2017), pp. 972–983. ISSN: 1573-062X. DOI: 10.1080/1573062X.2017.1279191. URL: <https://doi.org/10.1080/1573062X.2017.1279191> (visited on 10/11/2022).
- [10] Helena Mala-Jetmarova, Nargiz Sultanova, and Dragan Savic. “Lost in Optimisation of Water Distribution Systems? A Literature Review of System Design”. en. In: *Water* 10.3 (Mar. 2018), p. 307. ISSN: 2073-4441. DOI: 10.3390/w10030307. URL: <https://www.mdpi.com/2073-4441/10/3/307> (visited on 10/06/2022).
- [11] Sven Eggimann et al. “The Potential of Knowing More: A Review of Data-Driven Urban Water Management”. en. In: *Environmental Science & Technology* 51.5 (Mar. 2017), pp. 2538–2553. ISSN: 0013-936X, 1520-5851. DOI: 10.1021/acs.est.6b04267. URL: <https://pubs.acs.org/doi/10.1021/acs.est.6b04267> (visited on 10/26/2022).
- [12] Lewis A Rossman. “EPANET 2: users manual”. In: US Environmental Protection Agency. Office of Research and Development, 2000.
- [13] Vasso Reppa, Marios M. Polycarpou, and Christos G. Panayiotou. *Sensor fault diagnosis*. eng. Foundations and trends in systems and control 3, 1-2. Boston Delft Hanover: now publishers, 2016. ISBN: 9781680831283.
- [14] Zhirong Li et al. “Fast Detection and Localization of Multiple Leaks in Water Distribution Network Jointly Driven by Simulation and Machine Learning”. EN. In: *Journal of Water Resources Planning and Management* 148.9 (Sept. 2022), p. 05022005. ISSN: 1943-5452. DOI: 10.1061/(ASCE)WR.1943-5452.0001574. URL: <https://ascelibrary.org/doi/10.1061/%28ASCE%29WR.1943-5452.0001574> (visited on 01/27/2023).
- [15] David B. Steffelbauer et al. “Pressure-Leak Duality for Leak Detection and Localization in Water Distribution Systems”. EN. In: *Journal of Water Resources Planning and Management* 148.3 (Mar. 2022), p. 04021106. ISSN: 1943-5452. DOI: 10.1061/(ASCE)WR.1943-5452.0001515. URL: <https://ascelibrary.org/doi/10.1061/%28ASCE%29WR.1943-5452.0001515> (visited on 01/27/2023).
- [16] Xiaoting Wang et al. “Multiple Leakage Detection and Isolation in District Metering Areas Using a Multistage Approach”. EN. In: *Journal of Water Resources Planning and Management* 148.6 (June 2022), p. 04022021. ISSN: 1943-5452. DOI: 10.1061/(ASCE)WR.1943-5452.0001558. URL: <https://ascelibrary.org/doi/10.1061/%28ASCE%29WR.1943-5452.0001558> (visited on 01/26/2023).
- [17] Irene Marzola et al. “Leakage Detection and Localization in a Water Distribution Network through Comparison of Observed and Simulated Pressure Data”. EN. In: *Journal of Water Resources Planning and Management* 148.1 (Jan. 2022), p. 04021096. ISSN: 1943-5452. DOI: 10.1061/(ASCE)WR.1943-5452.0001503. URL: <https://ascelibrary.org/doi/10.1061/%28ASCE%29WR.1943-5452.0001503> (visited on 01/27/2023).
- [18] Ivo Daniel et al. “A Sequential Pressure-Based Algorithm for Data-Driven Leakage Identification and Model-Based Localization in Water Distribution Networks”. EN. In: *Journal of Water Resources Planning and Management* 148.6 (June 2022), p. 04022025. ISSN: 1943-5452. DOI: 10.1061/(ASCE)WR.1943-5452.0001535. URL: <https://ascelibrary.org/doi/10.1061/%28ASCE%29WR.1943-5452.0001535> (visited on 01/27/2023).

- [19] Daniele Laucelli et al. “Detecting anomalies in water distribution networks using EPR modelling paradigm”. en. In: *Journal of Hydroinformatics* 18.3 (May 2016), pp. 409–427. ISSN: 1464-7141, 1465-1734. DOI: 10.2166/hydro.2015.113. URL: <https://iwaponline.com/jh/article/18/3/409/3501/Detecting-anomalies-in-water-distribution-networks> (visited on 01/05/2023).
- [20] Michele Romano, Zoran Kapelan, and Dragan A. Savić. “Automated Detection of Pipe Bursts and Other Events in Water Distribution Systems”. EN. In: *Journal of Water Resources Planning and Management* 140.4 (Apr. 2014), pp. 457–467. ISSN: 1943-5452. DOI: 10.1061/(ASCE)WR.1943-5452.0000339. URL: <https://ascelibrary.org/doi/10.1061/%28ASCE%29WR.1943-5452.0000339> (visited on 01/05/2023).
- [21] Weirong Xu et al. “Disturbance Extraction for Burst Detection in Water Distribution Networks Using Pressure Measurements”. en. In: *Water Resources Research* 56.5 (May 2020). ISSN: 0043-1397, 1944-7973. DOI: 10.1029/2019WR025526. URL: <https://onlinelibrary.wiley.com/doi/10.1029/2019WR025526> (visited on 01/05/2023).
- [22] Donghui Jung et al. “Improving the rapidity of responses to pipe burst in water distribution systems: a comparison of statistical process control methods”. en. In: *Journal of Hydroinformatics* 17.2 (Mar. 2015), pp. 307–328. ISSN: 1464-7141, 1465-1734. DOI: 10.2166/hydro.2014.101. URL: <https://iwaponline.com/jh/article/17/2/307/3245/Improving-the-rapidity-of-responses-to-pipe-burst> (visited on 01/05/2023).
- [23] Dália Loureiro et al. “Water distribution systems flow monitoring and anomalous event detection: A practical approach”. en. In: *Urban Water Journal* 13.3 (Apr. 2016), pp. 242–252. ISSN: 1573-062X, 1744-9006. DOI: 10.1080/1573062X.2014.988733. URL: <http://www.tandfonline.com/doi/full/10.1080/1573062X.2014.988733> (visited on 01/05/2023).
- [24] Luis Romero-Ben et al. “Leak Localization in Water Distribution Networks Using Data-Driven and Model-Based Approaches”. EN. In: *Journal of Water Resources Planning and Management* 148.5 (May 2022), p. 04022016. ISSN: 1943-5452. DOI: 10.1061/(ASCE)WR.1943-5452.0001542. URL: <https://ascelibrary.org/doi/10.1061/%28ASCE%29WR.1943-5452.0001542> (visited on 01/27/2023).
- [25] Paul Dagum, Adam Galper, and Eric Horvitz. “Dynamic network models for forecasting”. In: *Uncertainty in artificial intelligence*. Elsevier, 1992, pp. 41–48.
- [26] Stuart J Russell. *Artificial intelligence a modern approach*. Pearson Education, Inc., 2010.
- [27] Judea Pearl. *Causality*. Cambridge university press, 2009.
- [28] Kun Zhang et al. “On estimation of functional causal models: general results and application to the post-nonlinear causal model”. In: *ACM Transactions on Intelligent Systems and Technology (TIST)* 7.2 (2015), pp. 1–22.
- [29] João Gama et al. “A Survey on Concept Drift Adaptation”. In: *ACM Comput. Surv.* 46.4 (Mar. 2014), 44:1–44:37. ISSN: 0360-0300.
- [30] F. Hinder, A. Artelt, and B. Hammer. “Towards Non-Parametric Drift Detection via Dynamic Adapting Window Independence Drift Detection (DAWIDD)”. In: *ICML*. 2020.

- [31] F Hinder et al. “Contrasting explanation of concept drift”. In: *30th European Symposium on Artificial Neural Networks, Computational Intelligence and Machine Learning, ESANN*. 2022.
- [32] Fabian Hinder et al. “Model-based explanations of concept drift”. In: *Neurocomputing* 555 (2023), p. 126640. ISSN: 0925-2312. DOI: <https://doi.org/10.1016/j.neucom.2023.126640>. URL: <https://www.sciencedirect.com/science/article/pii/S0925231223007634>.
- [33] Fabian Hinder and Barbara Hammer. “Feature Selection for Concept Drift Detection.” In: *ESANN*. Ed. by Michel Verleysen. 2023. URL: <https://pub.uni-bielefeld.de/record/2982830>.
- [34] Fabian Hinder and Barbara Hammer. “Concept Drift Segmentation via Kolmogorov Trees”. In: *Proceedings of the ESANN, 29th European Symposium on Artificial Neural Networks, Computational Intelligence and Machine Learning*. 2021.
- [35] Fabian Hinder et al. “Fast non-parametric conditional density estimation using moment trees”. In: *2021 IEEE Symposium Series on Computational Intelligence (SSCI)*. IEEE. 2021, pp. 1–7.
- [36] Rafael Izbicki and Ann B. Lee. “Converting high-dimensional regression to high-dimensional conditional density estimation”. In: (2017).
- [37] Inaam Ashraf et al. *Spatial Graph Convolution Neural Networks for Water Distribution Systems*. 2022. arXiv: 2211.09587 [cs.LG].

Table 2: Results of models for different metrics using geographical distances. The table shows median (m), mean (μ), and standard deviation (σ) over all 764 nodes and 42 runs. Bigger better (+), smaller better (-).

method	distance (-)		#closer(-)		rel. dist.(-)		best-3(+)	
	m	$\mu\pm\sigma$	m	$\mu\pm\sigma$	m	$\mu\pm\sigma$	m	$\mu\pm\sigma$
Random	1206.78	1347.67 \pm 783.45	14.0	13.96 \pm 8.36	7.53	11.76 \pm 13.60	0.0	0.31 \pm 0.51
Mean	730.66	837.70 \pm 586.64	7.0	7.88 \pm 6.29	4.27	6.90 \pm 8.04	1.0	0.71 \pm 0.77
FI (RF)	183.00	207.36 \pm 182.08	0.0	0.56 \pm 1.67	1.00	1.24 \pm 1.02	1.0	1.25 \pm 0.50
FI (ET)	180.22	204.29 \pm 170.32	0.0	0.52 \pm 1.51	1.00	1.23 \pm 0.99	2.0	1.83 \pm 0.59
PFI (ET)	180.22	203.08 \pm 153.39	0.0	0.51 \pm 1.30	1.00	1.22 \pm 0.90	2.0	1.89 \pm 0.60
PFI (RF)	183.00	205.33 \pm 159.14	0.0	0.53 \pm 1.35	1.00	1.23 \pm 0.92	1.0	1.30 \pm 0.52
SVM	212.39	435.81 \pm 647.79	0.0	3.50 \pm 7.96	1.00	3.01 \pm 6.28	2.0	1.50 \pm 0.78
LogR (I2)	295.26	659.34 \pm 685.25	1.0	6.53 \pm 8.69	1.31	5.07 \pm 7.91	1.0	1.23 \pm 0.97
LogR (I1)	268.50	627.08 \pm 711.75	1.0	5.99 \pm 8.80	1.09	4.85 \pm 8.23	1.0	1.19 \pm 0.89
FI (RF w/o DD)	211.07	460.35 \pm 612.80	0.0	4.48 \pm 8.44	1.00	2.70 \pm 3.95	1.0	0.96 \pm 0.54
FI (ET w/o DD)	195.34	359.68 \pm 513.24	0.0	2.89 \pm 7.16	1.00	2.08 \pm 3.10	1.0	1.24 \pm 0.67
PFI (RF w/o DD)	192.25	256.00 \pm 277.81	0.0	1.23 \pm 3.19	1.00	1.51 \pm 1.60	1.0	1.09 \pm 0.49
PFI (ET w/o DD)	242.40	502.63 \pm 523.98	0.0	4.65 \pm 6.67	1.00	3.03 \pm 3.84	1.0	0.73 \pm 0.53

A Additional Evaluation

In this section we present the evaluation and visualization that is not presented in the main paper due to space restrictions.

A.1 Overview

We present the results for the different metrics, similar to Table 1, if computed with geometrical distance rather than topological in Table 2. Furthermore, the results for all metrics and both distance measures are visualised in Figure 6.

Furthermore, we visualized rank statistics in of all methods over all runs and pipes in Figures 7 and 8 using all metrics based on both distances. In Figure 7 we used the Bonferroni-Dunn statistic ($\alpha = 0.05$) to show that all results are better than the Random baseline, in Figure 8 we used the Nemenyi statistic ($\alpha = 0.05$) to show significant differences between the methods. In both cases we assumed that the pipes are sufficiently different.

A.2 Network Visualization

We visualized the network for all methods and metrics, using both distances. The colors are normalized so that purple indicates best and yellow worst outcome. More specifically we used the following normalizations:

- best-3 was absolute normalized (best: 3, worst: 0).
- distance was normalized with respect to globally worst outcome, taking different base distances (topological vs. geographical) into account (best: 0, worst: maximum over all pipes and methods)
- #closer was normalized similar to distance (best: 0, worst: maximum over all pipes and methods)
- rel. dist. was normalized between the closest sensor (best possible) and the Random baseline (best: closes sensor, worst: Random baseline)

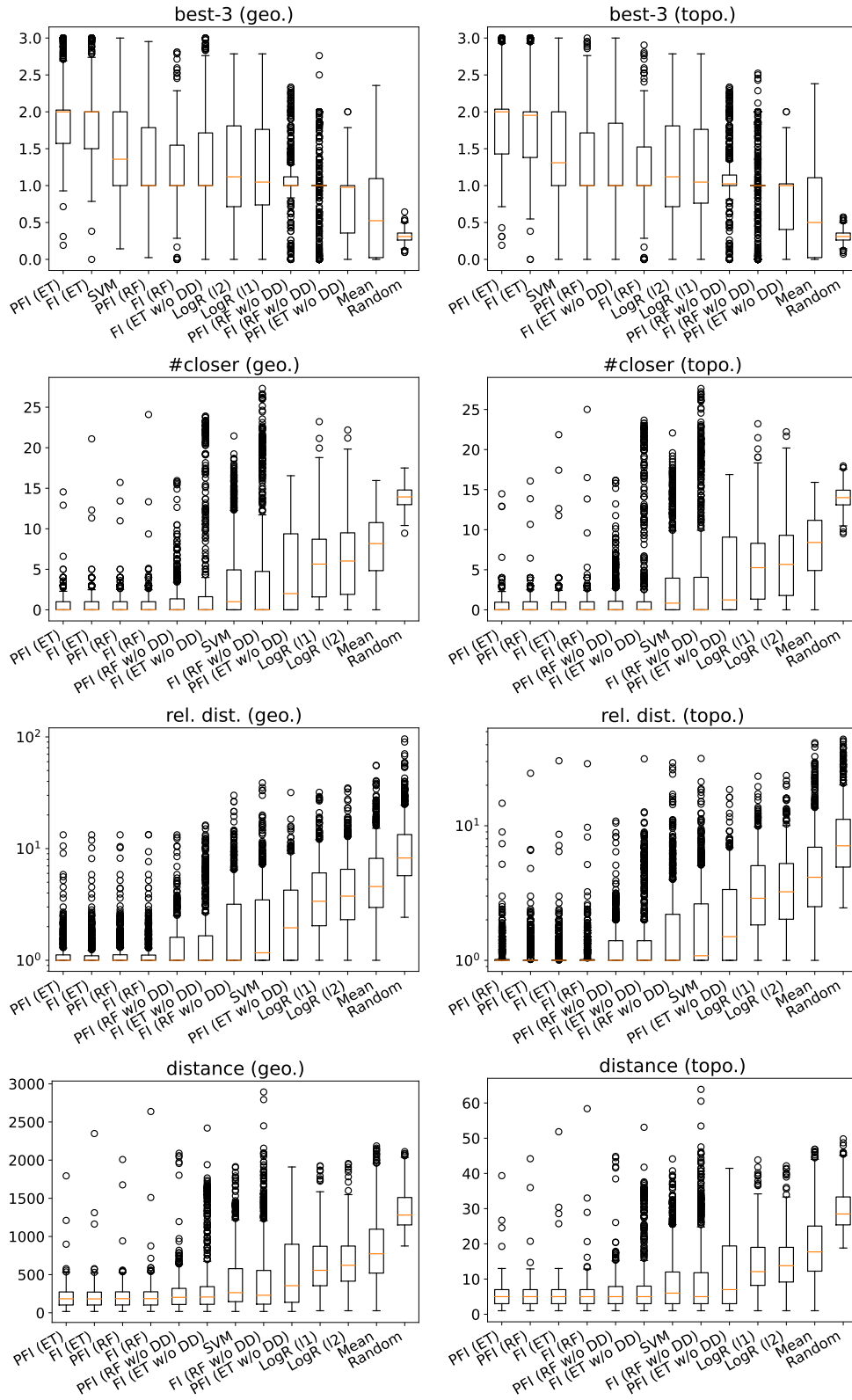


Figure 6: Visualization of metrics for all methods using both distances. Each point corresponds to the mean over all runs on a single pipe. Boxes are ordered according to mean value, starting from best going to worst.

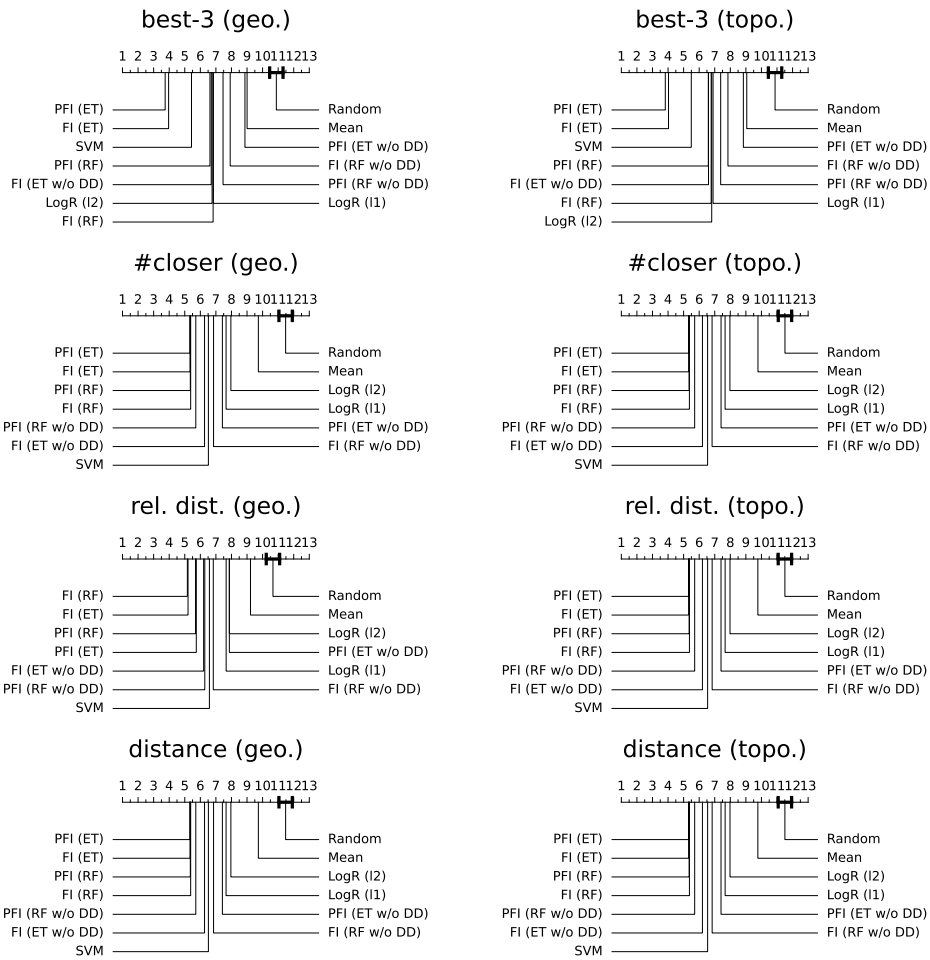


Figure 7: Method ranking based on different metrics and distances. Bonferroni-Dunn test was used to show significant difference to the Random baseline.

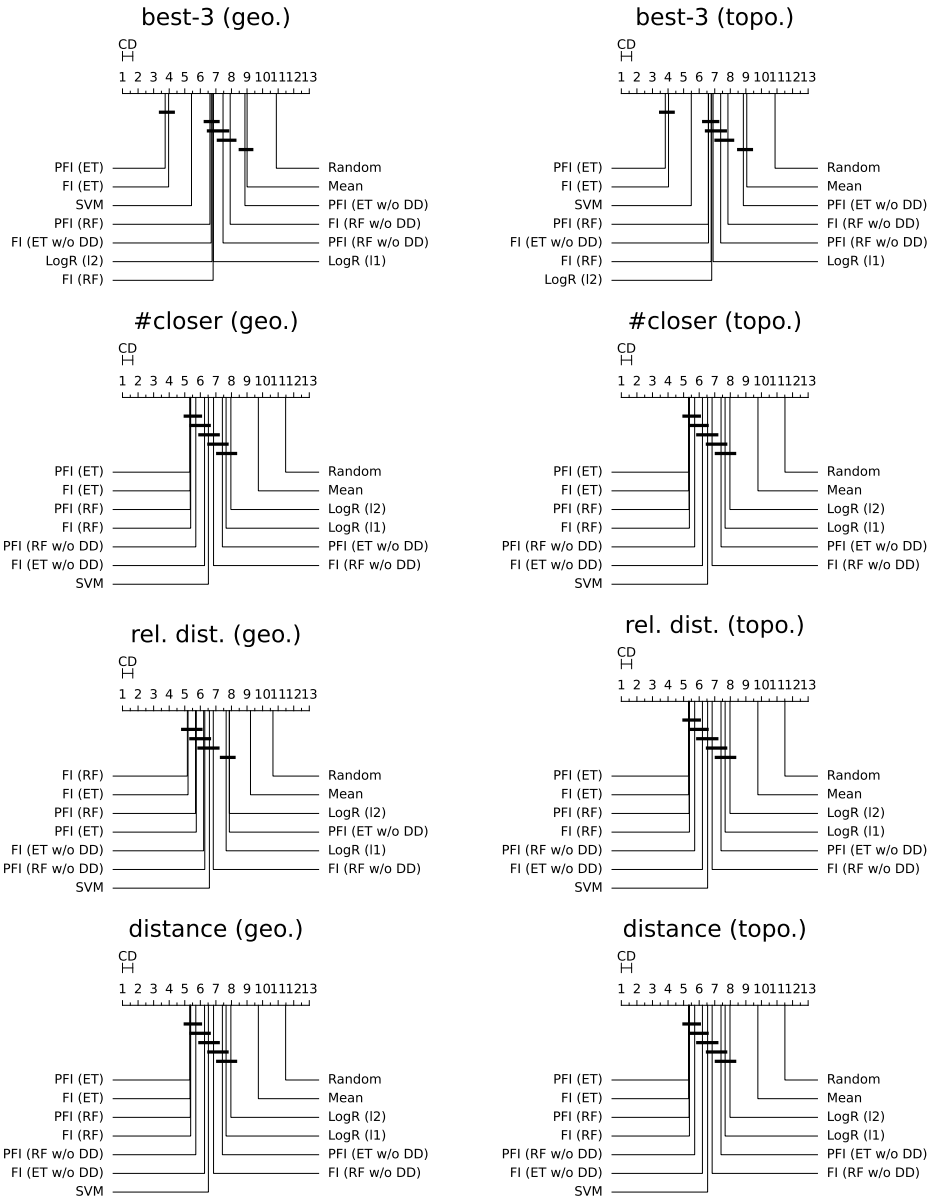
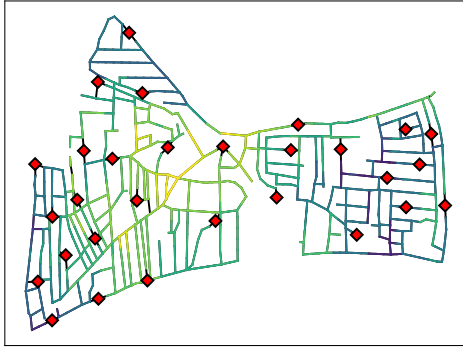
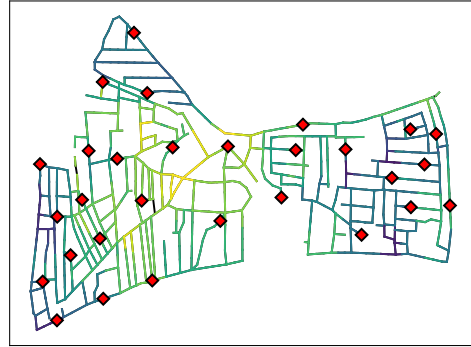


Figure 8: Method ranking based on different metrics and distances. Nemenyi's test was used to show significant difference between methods.

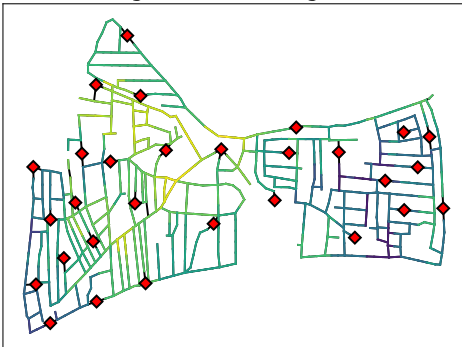
LogR (l2) best-3 (geo.)



LogR (l2) best-3 (topo.)



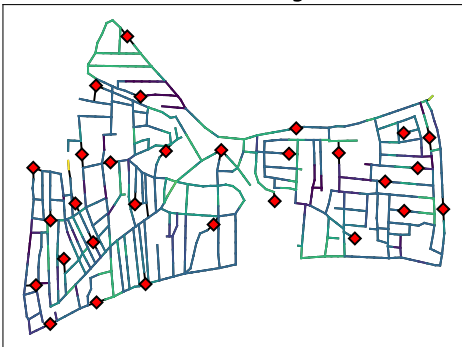
LogR (l1) best-3 (geo.)



LogR (l1) best-3 (topo.)



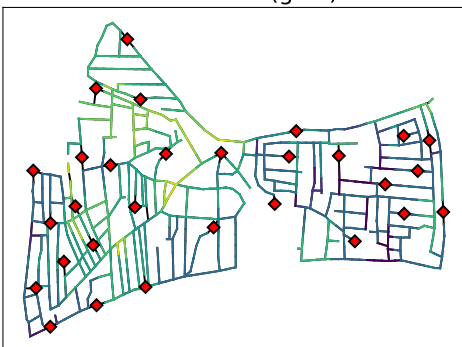
FI (ET) best-3 (geo.)



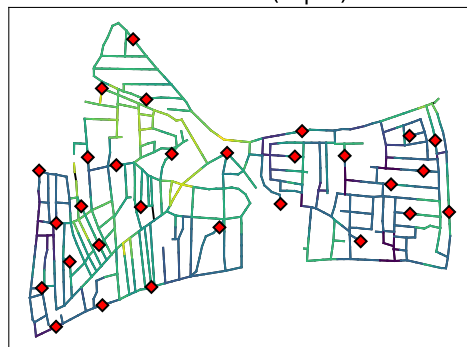
FI (ET) best-3 (topo.)



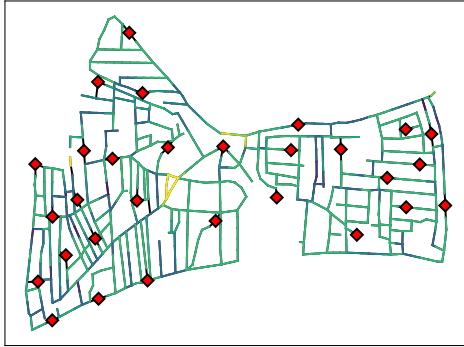
SVM best-3 (geo.)



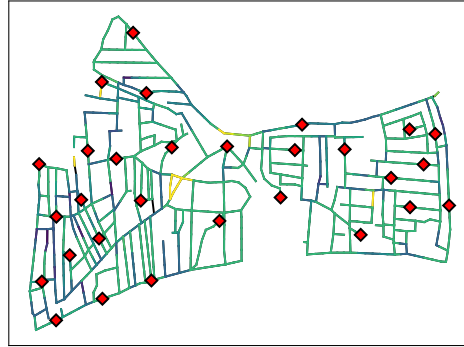
SVM best-3 (topo.)



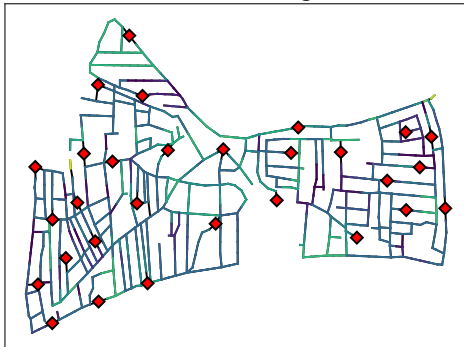
FI (RF) best-3 (geo.)



FI (RF) best-3 (topo.)



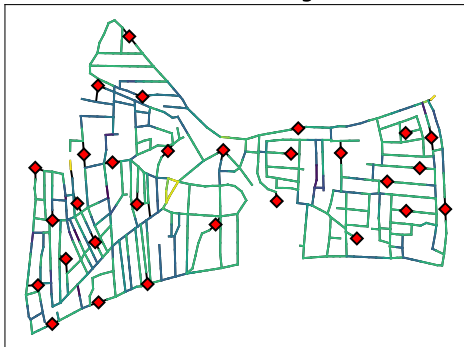
PFI (ET) best-3 (geo.)



PFI (ET) best-3 (topo.)



PFI (RF) best-3 (geo.)



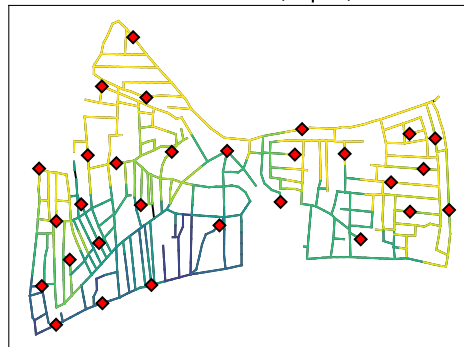
PFI (RF) best-3 (topo.)



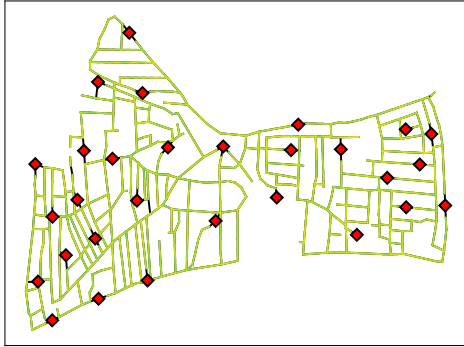
Mean best-3 (geo.)



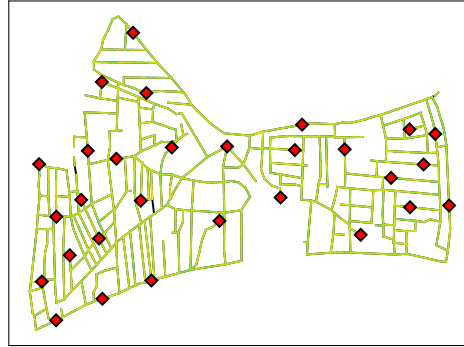
Mean best-3 (topo.)



Random best-3 (geo.)



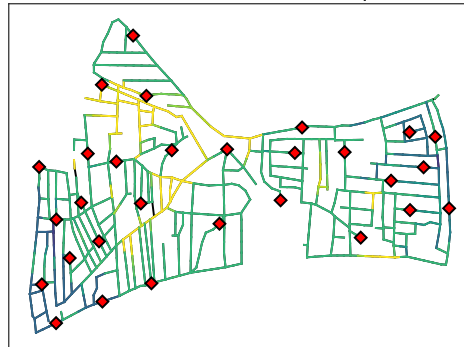
Random best-3 (topo.)



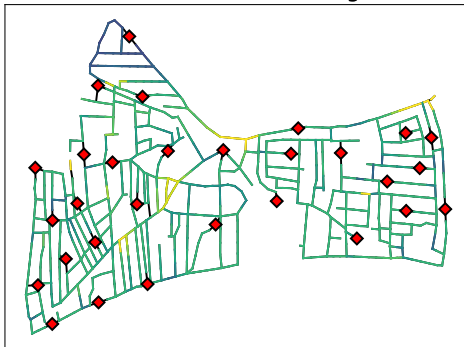
FI (RF w/o DD) best-3 (geo.)



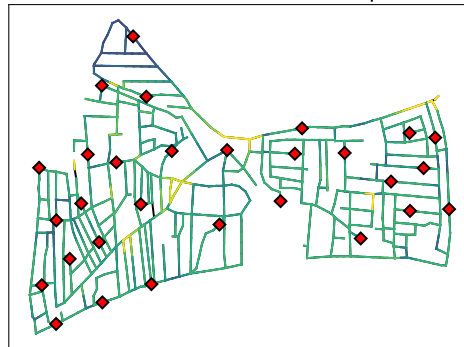
FI (RF w/o DD) best-3 (topo.)



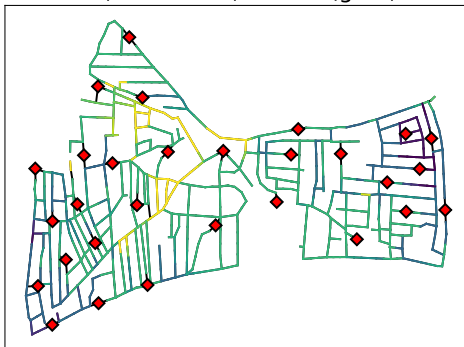
PFI (RF w/o DD) best-3 (geo.)



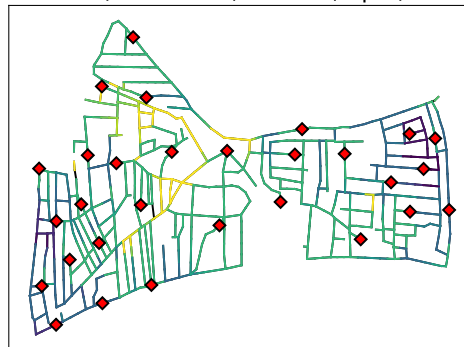
PFI (RF w/o DD) best-3 (topo.)



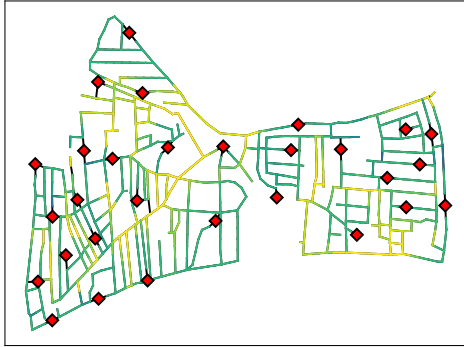
FI (ET w/o DD) best-3 (geo.)



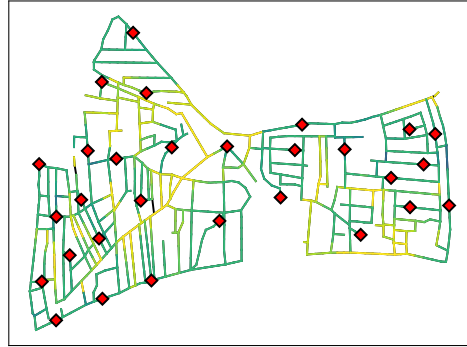
FI (ET w/o DD) best-3 (topo.)



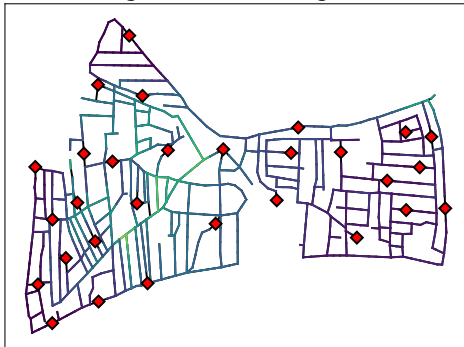
PFI (ET w/o DD) best-3 (geo.)



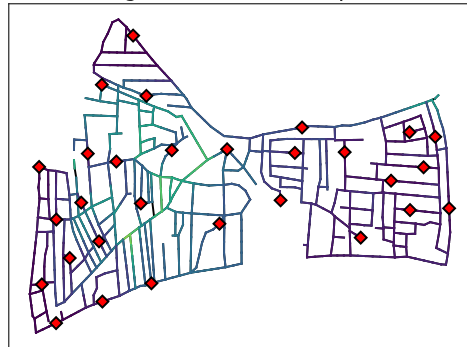
PFI (ET w/o DD) best-3 (topo.)



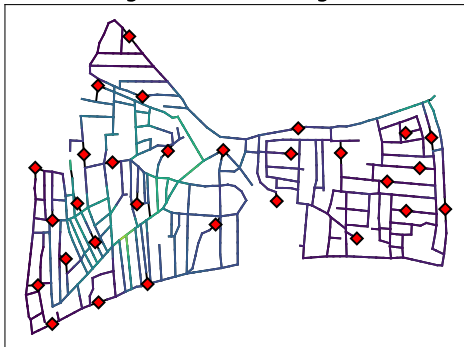
LogR (I2) #closer (geo.)



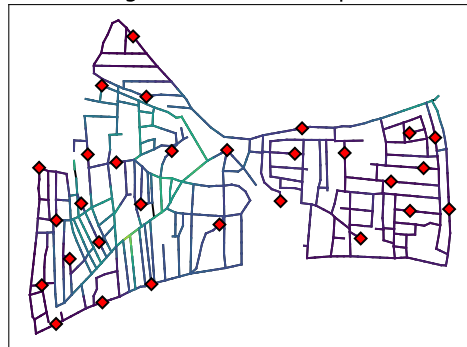
LogR (I2) #closer (topo.)



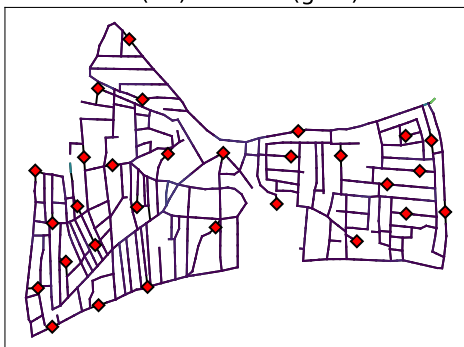
LogR (I1) #closer (geo.)



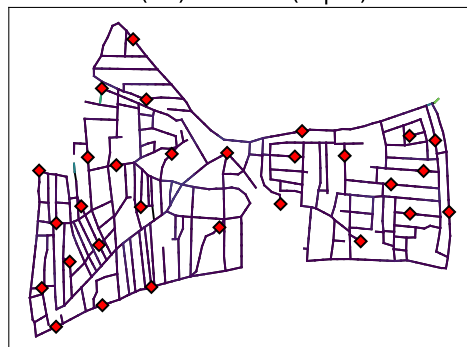
LogR (I1) #closer (topo.)



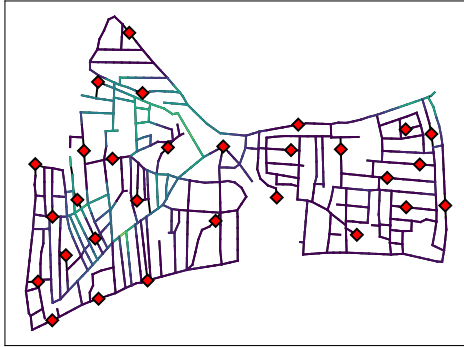
FI (ET) #closer (geo.)



FI (ET) #closer (topo.)



SVM #closer (geo.)



SVM #closer (topo.)



FI (RF) #closer (geo.)



FI (RF) #closer (topo.)



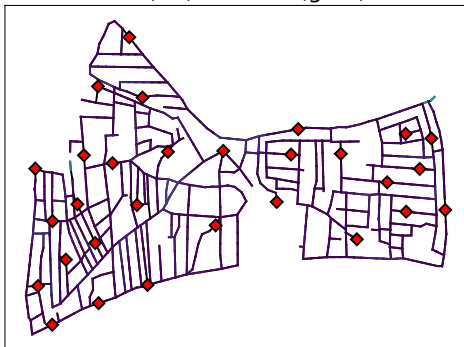
PFI (ET) #closer (geo.)



PFI (ET) #closer (topo.)

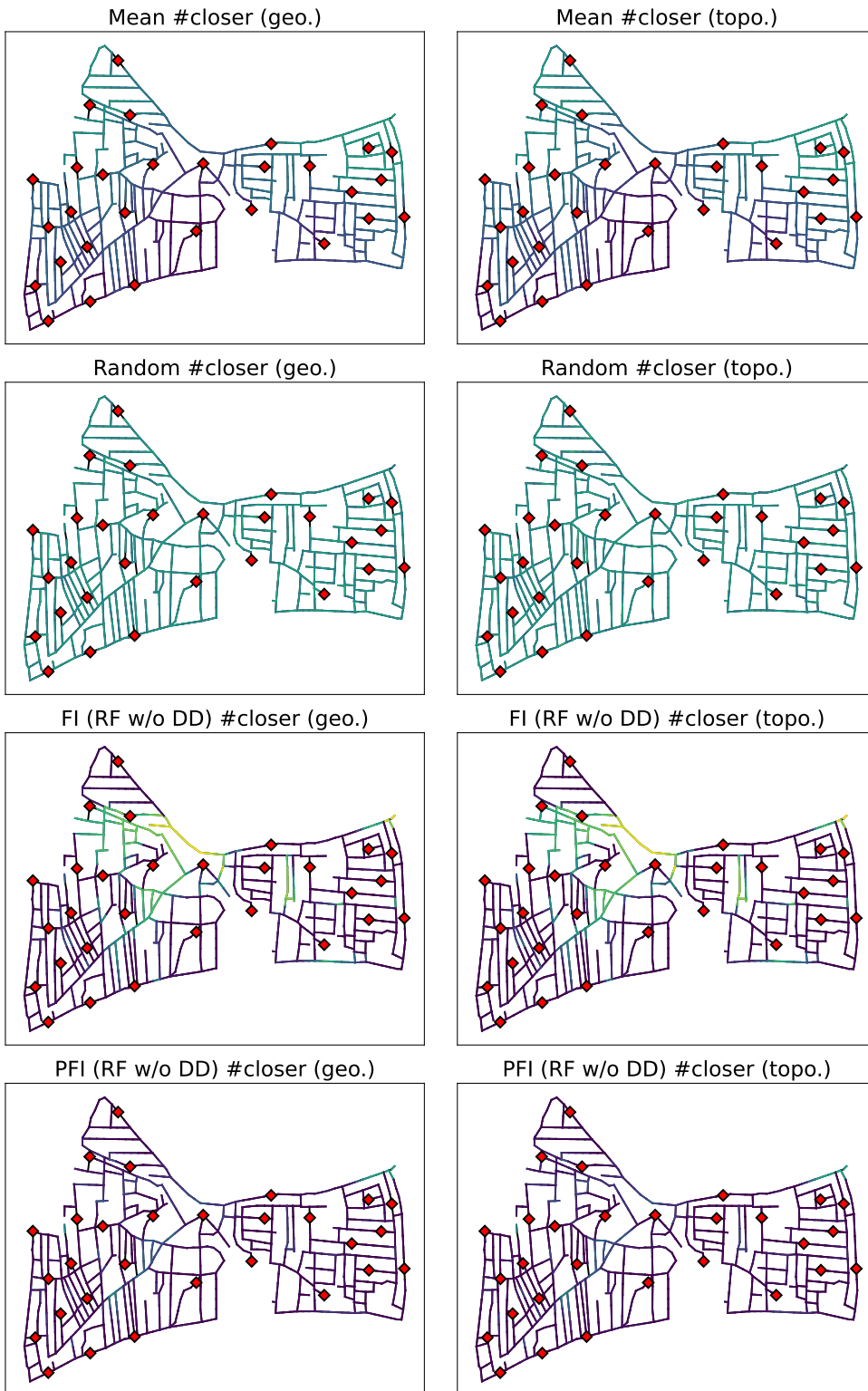


PFI (RF) #closer (geo.)

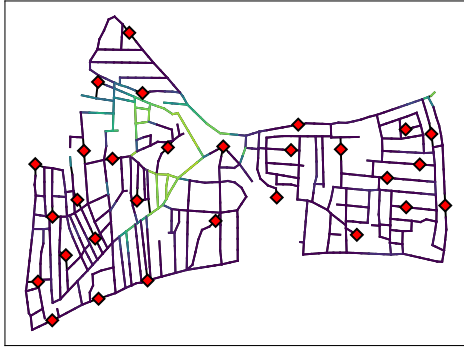


PFI (RF) #closer (topo.)





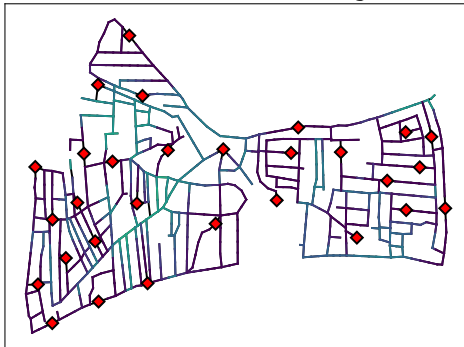
FI (ET w/o DD) #closer (geo.)



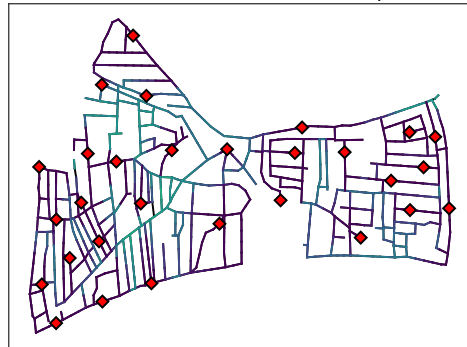
FI (ET w/o DD) #closer (topo.)



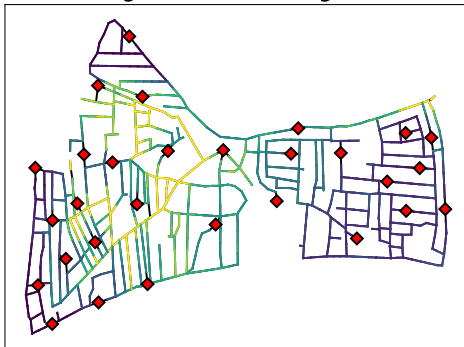
PFI (ET w/o DD) #closer (geo.)



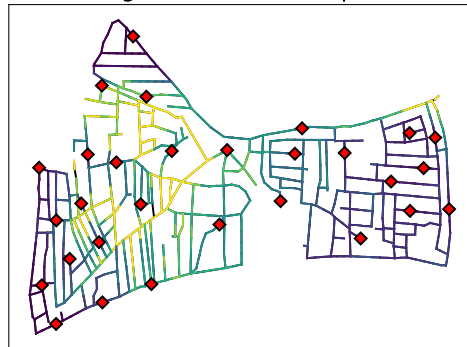
PFI (ET w/o DD) #closer (topo.)



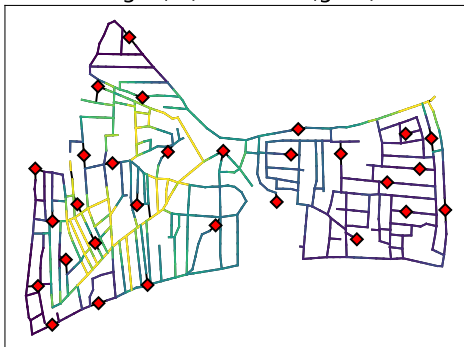
LogR (l2) rel. dist. (geo.)



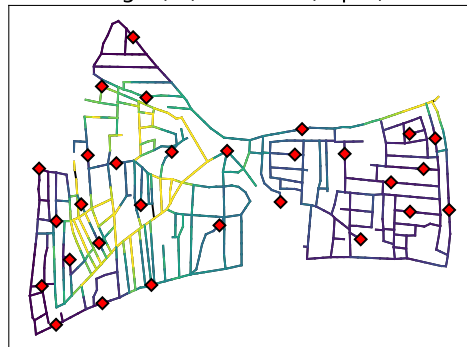
LogR (l2) rel. dist. (topo.)



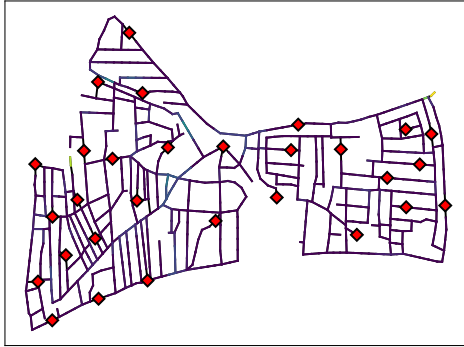
LogR (l1) rel. dist. (geo.)



LogR (l1) rel. dist. (topo.)



FI (ET) rel. dist. (geo.)



FI (ET) rel. dist. (topo.)



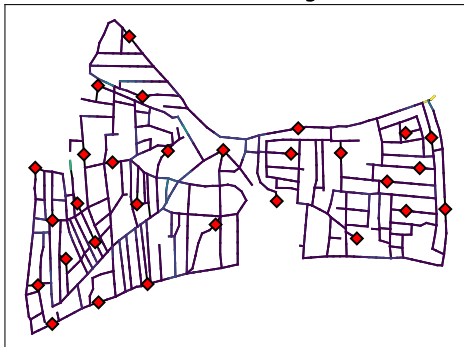
SVM rel. dist. (geo.)



SVM rel. dist. (topo.)



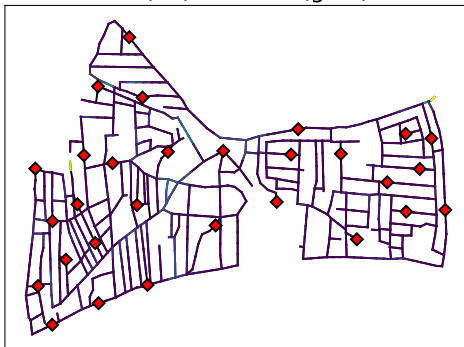
FI (RF) rel. dist. (geo.)



FI (RF) rel. dist. (topo.)



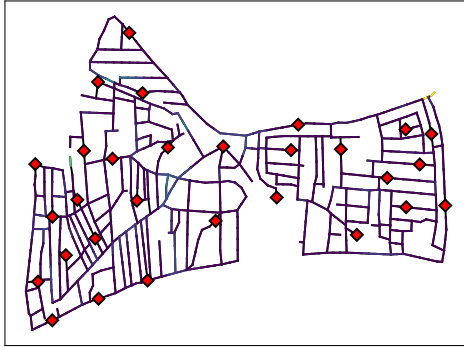
PFI (ET) rel. dist. (geo.)



PFI (ET) rel. dist. (topo.)



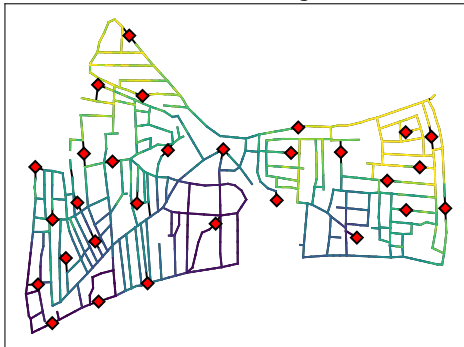
PFI (RF) rel. dist. (geo.)



PFI (RF) rel. dist. (topo.)



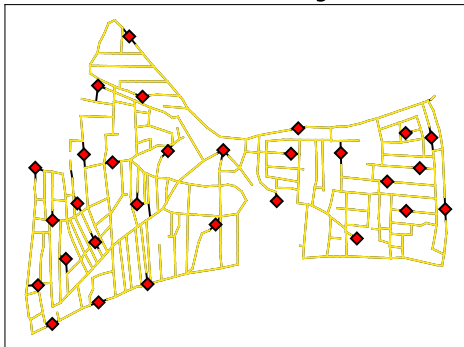
Mean rel. dist. (geo.)



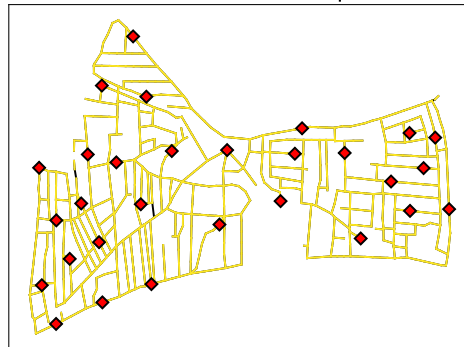
Mean rel. dist. (topo.)



Random rel. dist. (geo.)



Random rel. dist. (topo.)



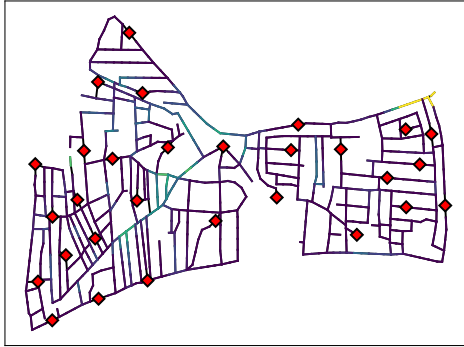
FI (RF w/o DD) rel. dist. (geo.)



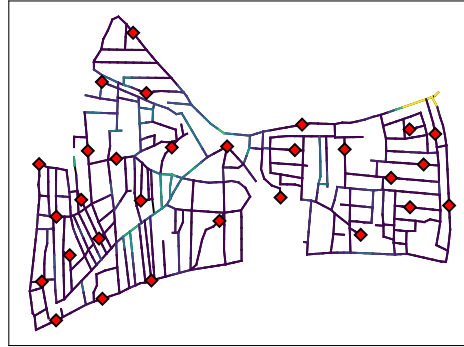
FI (RF w/o DD) rel. dist. (topo.)



PFI (RF w/o DD) rel. dist. (geo.)



PFI (RF w/o DD) rel. dist. (topo.)



FI (ET w/o DD) rel. dist. (geo.)



FI (ET w/o DD) rel. dist. (topo.)



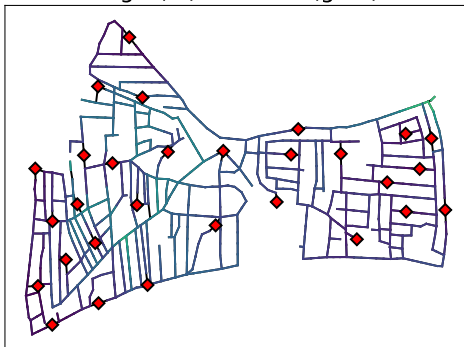
PFI (ET w/o DD) rel. dist. (geo.)



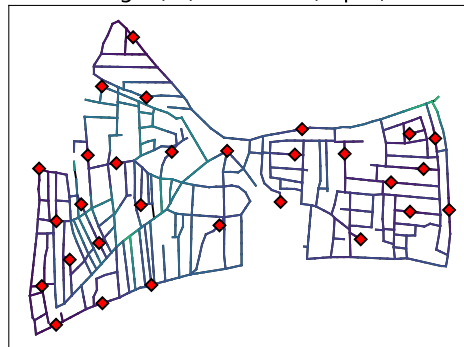
PFI (ET w/o DD) rel. dist. (topo.)



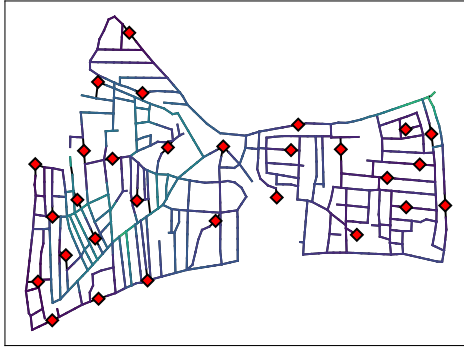
LogR (I2) distance (geo.)



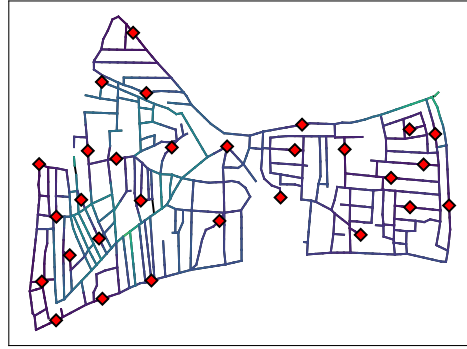
LogR (I2) distance (topo.)



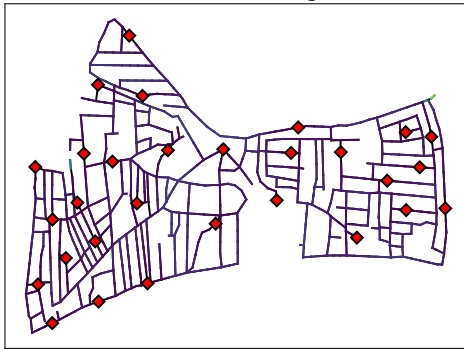
LogR (l1) distance (geo.)



LogR (l1) distance (topo.)



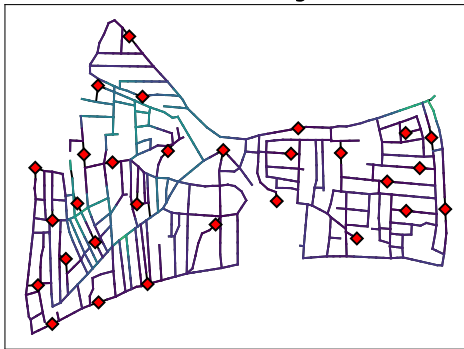
FI (ET) distance (geo.)



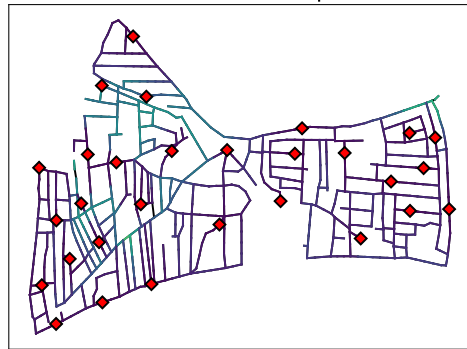
FI (ET) distance (topo.)



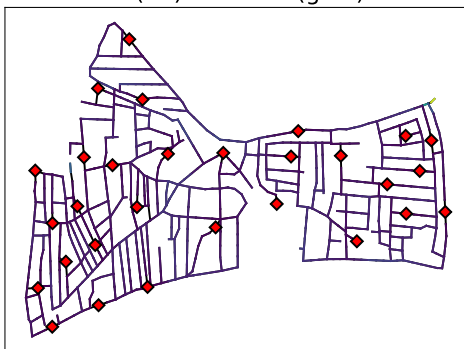
SVM distance (geo.)



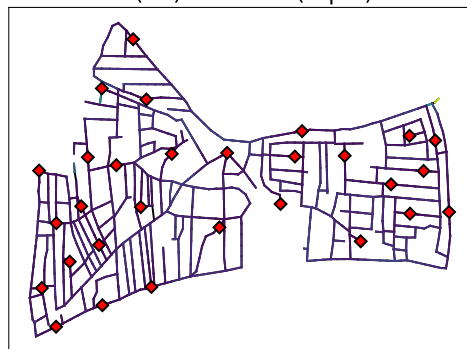
SVM distance (topo.)



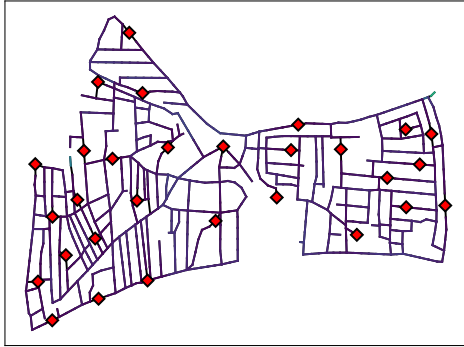
FI (RF) distance (geo.)



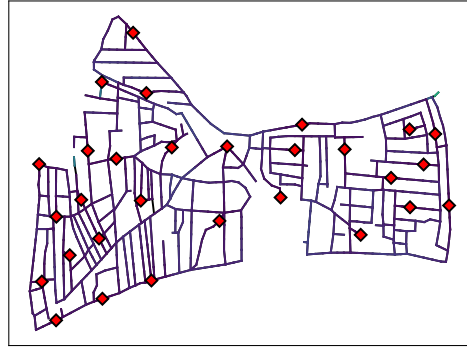
FI (RF) distance (topo.)



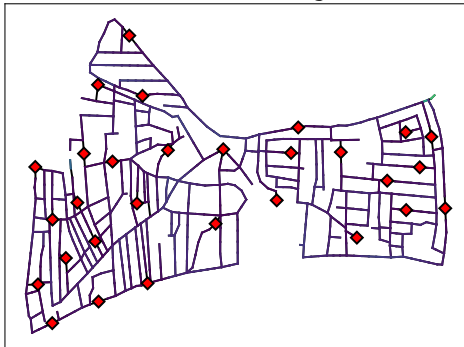
PFI (ET) distance (geo.)



PFI (ET) distance (topo.)



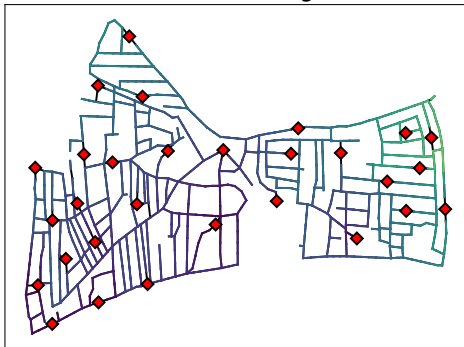
PFI (RF) distance (geo.)



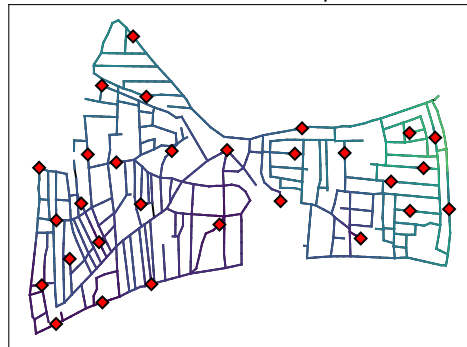
PFI (RF) distance (topo.)



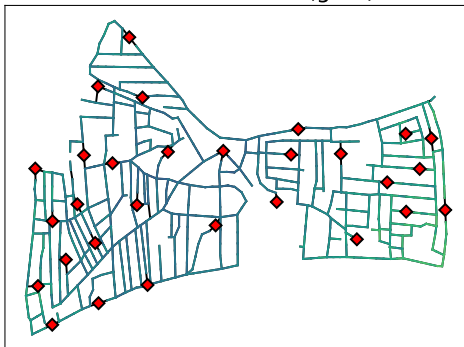
Mean distance (geo.)



Mean distance (topo.)



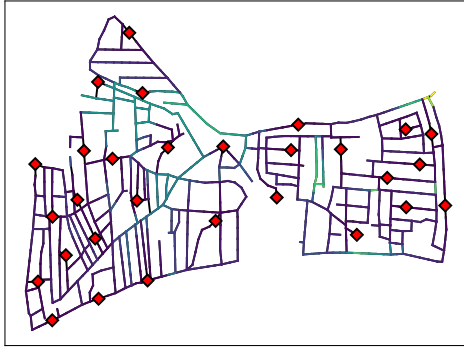
Random distance (geo.)



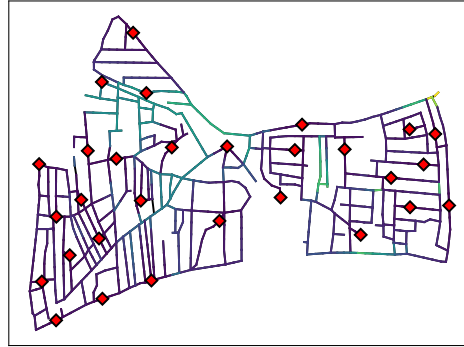
Random distance (topo.)



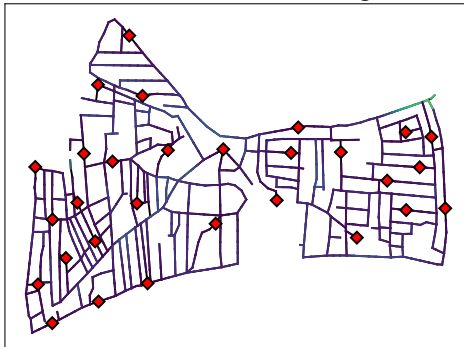
FI (RF w/o DD) distance (geo.)



FI (RF w/o DD) distance (topo.)



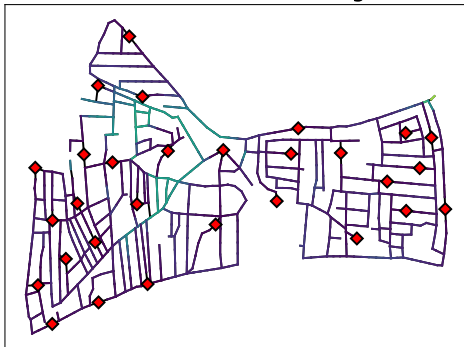
PFI (RF w/o DD) distance (geo.)



PFI (RF w/o DD) distance (topo.)



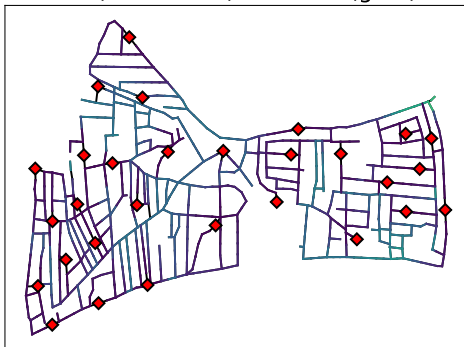
FI (ET w/o DD) distance (geo.)



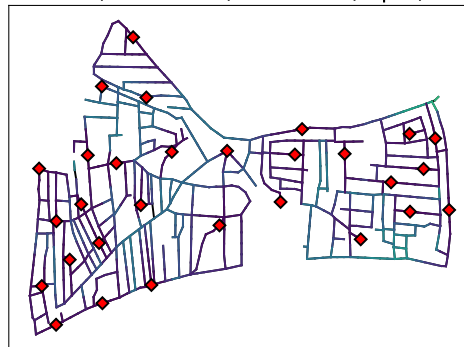
FI (ET w/o DD) distance (topo.)



PFI (ET w/o DD) distance (geo.)



PFI (ET w/o DD) distance (topo.)



B Proofs

Lemma 1. Let $D : \mathbb{Z} \rightarrow \mathbb{R}^{V(G)}, t \mapsto D_t$ be a demand pattern and assume that the transition function $P(\cdot, d)$ is uniformly Lipschitz continuous for all $d \in \mathbb{R}^{V(G)}$, i.e. we have $\sup_{d \in \mathbb{R}^{V(G)}} \|P(p, d) - P(p', d)\|_1 \leq C_s \|p - p'\|_1$, with constant $C_s < 1$. Then for every time-point t_0 it holds that P has exactly one fix-point, i.e. there exists exactly one $p \in \mathbb{R}^{V(G)}$ such that $p = P(p, D_{t_0})$.

Furthermore, denote by $P_0^{(t_0)}(p, D.) = p$, $P_{t+1}^{(t_0)}(p, D.) = P_t^{(t_0+1)}(P(p, D_{t_0}), D.)$. Then $P_t^{(t_0)}(p, D.)$ becomes independent of the choice of p and t_0 as time passes by, i.e. for all $p, p' \in \mathbb{R}^{V(G)}$ and $M \in \mathbb{Z}_{\geq 0}$ we have

$$\|P_t^{(t_0)}(p, D.) - P_{t+M}^{(t_0-M)}(p', D.)\|_1 \rightarrow 0 \text{ as } t - t_0 \rightarrow \infty.$$

In particular, $t \mapsto P_t(D.) := \lim_{n \rightarrow \infty} P_{t+n}^{(-n)}(p, D.)$ is well defined and constant for constant demand patterns $D. = D$.

Proof. For the first statement proceed as in the proof of Banach's fix-point theorem using that as t_0 is fixed $P(\cdot, D_{t_0})$ is a contraction of $\mathbb{R}^{V(G)}$ onto itself.

Now, prove the second statement: We apply the same argument as used in Banach's fix-point theorem. To do so first notice that we can rewrite $P_{t+1}^{(t_0)}(p, D.) = P(P_t^{(t_0)}(p, D.), D_{t_0+t})$ and hence

$$\begin{aligned} & \|P_t^{(t_0)}(p, D.) - P_{t+M}^{(t_0-M)}(p', D.)\|_1 \\ &= \|P(P_{t-1}^{(t_0)}(p, D.), D_{t_0+t-1}) - P(P_{t+M-1}^{(t_0-M)}(p', D.), D_{t_0-M+t+M-1})\|_1 \\ &\leq C_s \|P_{t-1}^{(t_0)}(p, D.) - P_{t+M-1}^{(t_0-M)}(p', D.)\|_1 \\ &\leq \dots \leq C_s^{t-t_0} \underbrace{\|p - P_M^{(t_0-M)}(p', D.)\|_1}_{\leq K} \xrightarrow{t \rightarrow \infty} 0. \end{aligned}$$

□

Lemma 2. Assume that the transition function P is Lipschitz continuous in the first and α -Hölder continuous second argument, i.e. $\|P(p, d) - P(p', d')\|_1 \leq C_s \|p - p'\|_1 + C_d \|d - d'\|_1^\alpha$ with $C_s < 1$. Then it holds:

1. For constant demands, the pressures are α -Hölder continuous with constant $C_d/(1 - C_s)$.
2. The pressures of a stochastic demand pattern are approximated by the pressures of the mean demand pattern up to $C_d/(1 - C_s)$ times the α^{th} -power of the sum of the demand wise standard deviations.

Proof. 1.: Let D, D' be arbitrary demands. It holds

$$\begin{aligned} \|P(D) - P(D')\|_1 &= \|P(P(D), D) - P(P(D'), D')\|_1 \\ &\leq C_s \|P(D) - P(D')\|_1 + C_d \|D - D'\|_1^\alpha \\ &\leq \dots \leq \underbrace{C_s^{n+1}}_{\rightarrow 0} \|P(D) - P(D')\|_1 + \underbrace{\left(\sum_{i=0}^n C_s^i \right)}_{\rightarrow 1/(1-C_s)} C_d \|D - D'\|_1^\alpha \\ &\xrightarrow{n \rightarrow \infty} \frac{C_d}{1 - C_s} \|D - D'\|_1^\alpha. \end{aligned}$$

Thus for every bounded set of demands the function is locally α -Hölder continuous. As the constant, in contrast to the rate of convergence, does not depend on the demands, the function is α -Hölder continuous.

2.: Let $D : \Omega \rightarrow \mathbb{R}^{V(G)}$ be a stochastic demand pattern with component wise mean $\mu = \mathbb{E}[D]$ (this is well defined as $|V(G)|$ is finite). Then it holds

$$\|P(D(\omega)) - P(\mu)\|_1 \stackrel{1.}{\leq} \frac{C_d}{1 - C_s} \|D(\omega) - \mu\|_1^\alpha.$$

Taking expectation on both sides and using that $0 < \alpha \leq 1$ so that x^α is concave on $\mathbb{R}_{\geq 0}$ we have by using Jensen's inequality applied twice

$$\begin{aligned} \|P(D) - P(\mu)\|_{L^1} &\leq \frac{C_d}{1 - C_s} (\mathbb{E}[\|D - \mu\|_1])^\alpha \\ &= \frac{C_d}{1 - C_s} \left(\sum_{v \in V(G)} \mathbb{E}[\|D_v - \mu_v\|] \right)^\alpha \\ &\leq \frac{C_d}{1 - C_s} \left(\sum_{v \in V(G)} \sqrt{\mathbb{E}[(D_v - \mu_v)^2]} \right)^\alpha \\ &= \frac{C_d}{1 - C_s} \left(\sum_{v \in V(G)} \text{Std}(D_v) \right)^\alpha. \end{aligned}$$

□

Of Theorem 1. If w and v are not connected in G , then $d_G(w, v) = \infty$ and by the definition of the transition function, L does not affect $P(D + L)$ so that the difference is 0 and the inequality is fulfilled.

Thus, assume G is connected. Denote by $\Delta_u = |(P(D))_u - (P(D + L))_u|$, by $\Delta(n) = \sup_{d_G(v, u) = n} \Delta_u$, by $N(u)$ the set of all neighbours of u in G . By convention we set $\sup \emptyset = -\infty$. Then we have

$$\begin{aligned} \Delta(n) &= \sup_{d_G(v, u) = n} \Delta_u \leq \sup_{d_G(v, u) = n} C_s \left(\Delta_u + \sum_{u' \in N(u)} \Delta_{u'} \right) + C_d \cdot \delta_{uv} l^\alpha \\ &\leq C_s (\deg G + 1) \max\{\Delta(n - 1), \Delta(n), \Delta(n + 1)\} + \mathbf{1}[n = 0] C_d l^\alpha, \end{aligned}$$

where the last inequality holds since every node is affected by its at most $\deg G$ neighbors and itself and each of those is at most 1 node closer or further away from v than u .

Now, show that $\Delta(n)$ is decreasing: For $n \geq 1$ we have

$$\Delta(n) \leq C_s (\deg G + 1) \max\{\Delta(n - 1), \Delta(n), \Delta(n + 1)\}$$

As $C_s (\deg G + 1) < 1$ the maximum on the right-hand side is bigger than $\Delta(n)$, in particular, it has to be given by either $\Delta(n + 1)$ or $\Delta(n - 1)$. If we apply this argument inductively, starting at $N = \sup_{u \in V(G)} d_G(u, v)$ so that $\Delta(N + 1) = -\infty$ we see that

$$\Delta(N) \leq \Delta(N - 1) \leq \dots \leq \Delta(2) \leq \Delta(1) \leq \Delta(0),$$

as all $\Delta(n) \geq 0$ and where the last term is obtained by applying the argument to $n = 1$. Thus, by induction, we have

$$\Delta(n) \leq (C_s (\deg G + 1))^n \Delta(0).$$

In particular, equality for $\Delta(1)$ holds if and only if $\Delta(0) = 0$.

For $n = 0$ we have that each neighbour has distance 1 from v thus we have

$$\begin{aligned}\Delta(0) &\leq C_s \Delta(0) + C_s \deg G \Delta(1) + C_d l^\alpha \\ &< C_s (\deg G + 1) \Delta(0) + C_d l^\alpha \\ \Rightarrow \Delta(n) &< \frac{C_d l^\alpha (C_s (\deg G + 1))^n}{1 - C_s (\deg G + 1)}.\end{aligned}$$

Here the strict inequality follows by the fact $\Delta(0) \geq C_d l^\alpha > 0$.

Necessity: Consider $G = (\{v, w, u_1, \dots, u_n\}, \{v, w\} \times \{u_1, \dots, u_n\})$, $P_v(p, d) = d$, $P_{u_i}(p, d) = C_s p_v$, $P_w(p, d) = C_s \sum_i p_{u_i}$. Then $|P_v(p, d) - P_v(p', d')| \leq |d - d'|$, $|P_{u_i}(p, d) - P_{u_i}(p', d')| = C_s |p_v - p'_v|$, $|P_w(p, d) - P_w(p', d')| = C_s |\sum_{i=1}^n p_{u_i} - p'_{u_i}| \leq C_s \sum_{i=1}^n |p_{u_i} - p'_{u_i}|$ so the transition function fulfills the requirements. However,

$$\begin{aligned}(P(D))_{u_i} &= C_s (P(D))_v = C_s D_v \\ (P(D))_w &= C_s \sum_{i=1}^n (P(D))_{u_i} = n C_s^2 D_v\end{aligned}$$

and thus

$$\frac{|(P(D))_w - (P(D+L))_w|}{|(P(D))_{u_i} - (P(D+L))_{u_i}|} = \frac{n C_s^2 l}{C_s l} = n C_s$$

as $\deg G = n$ the statement follows. \square